



Article

<https://doi.org/10.1038/s41591-025-03574-1>

Microglial mechanisms drive amyloid- β clearance in immunized patients with Alzheimer's disease

Received: 5 April 2024**A list of authors and their affiliations appears at the end of the paper**

Accepted: 6 February 2025

Published online: 6 March 2025

 Check for updates

Alzheimer's disease (AD) therapies utilizing amyloid- β (A β) immunization have shown potential in clinical trials. Yet, the mechanisms driving A β clearance in the immunized AD brain remain unclear. Here, we use spatial transcriptomics to explore the effects of both active and passive A β immunization in the AD brain. We compare actively immunized patients with AD with nonimmunized patients with AD and neurologically healthy controls, identifying distinct microglial states associated with A β clearance. Using high-resolution spatial transcriptomics alongside single-cell RNA sequencing, we delve deeper into the transcriptional pathways involved in A β removal after lecanemab treatment. We uncover spatially distinct microglial responses that vary by brain region. Our analysis reveals upregulation of the triggering receptor expressed on myeloid cells 2 (*TREM2*) and apolipoprotein E (*APOE*) in microglia across immunization approaches, which correlate positively with antibody responses and A β removal. Furthermore, we show that complement signaling in brain myeloid cells contributes to A β clearance after immunization. These findings provide new insights into the transcriptional mechanisms orchestrating A β removal and shed light on the role of microglia in immune-mediated A β clearance. Importantly, our work uncovers potential molecular targets that could enhance A β -targeted immunotherapies, offering new avenues for developing more effective therapeutic strategies to combat AD.

For nearly three decades, clinical trials have targeted cerebral A β accumulation in AD¹. Leading strategies include active and passive immunization against A β ². While these strategies can reduce cerebral A β ^{3–9}, they can also trigger adverse side effects^{8–15}. Understanding the cellular mechanisms underpinning A β immunization is paramount to improving patient outcomes.

The AN1792 clinical trial was the first to actively immunize patients with AD³. This trial utilized immunization against a synthetic A $\beta_{1–42}$ peptide. Preclinical studies showed promise, but the trial was suspended after some patients developed aseptic meningoencephalitis^{10–12} associated with cerebral amyloid angiopathy (CAA)^{4,13}. Our prior

postmortem analyses of AN1792 brains revealed A β clearance in some immunized patients, likely via microglia^{3–5,16}. However, the microglial mechanisms dictating A β clearance in these brains remain unclear.

The inflammatory side effects from the AN1792 trial led to a shift toward passive immunization. In passive immunization, patients with AD receive antibodies that target A β , such as lecanemab. Lecanemab binds large soluble A β protofibrils, reduces A β markers and slows cognitive decline in early AD⁹. Our prior case study of a lecanemab-treated patient who developed stroke-like symptoms revealed inflammation in blood vessels with CAA and evidence of A β clearance^{17,18}. Yet, the

function of microglia in A β clearance in passive immunization also remains unclear.

In this study, we used spatial transcriptomics (ST) to analyze the neuroimmune response in AD brains following active and passive A β immunization. We compared AN1792-immunized Alzheimer's disease (iAD) brains to nonimmunized Alzheimer's disease (nAD) and control, non-neurologic disease (NND) brains. Additionally, we examined the neuroimmune response in the aforementioned patient treated with lecanemab using high-definition ST, spatial proteogenomics and single-cell RNA sequencing (scRNA-seq).

Our study uncovers distinct microglial phenotypes in A β -immunized AD brains and reveals genes that control clearance of A β by microglia. These results highlight candidate genes to modulate microglial responses in AD immunotherapy.

Results

Active A β immunization sustains inflammation at the A β niche

We utilized ST to analyze brain frontal cortex (FCX) sections of patients with AD from the AN1792 trial (Fig. 1a). This cohort included 13 iAD brains, as well as 6 nAD and 6 NND control brains (Fig. 1b). Extended Data Table 1 details the clinical and pathologic profiles of these individuals. Groups were age matched (Fig. 1c) and sex matched (Extended Data Fig. 1a). A 6.5×6.5 -mm ST capture area (4,992 spots) was analyzed, and ST spots were manually annotated by cortical layers, meninges or white matter using H&E staining (Fig. 1d). No significant differences were found in ST spot or feature counts per region (Extended Data Fig. 1b,c). Cortical layer I of iAD samples showed lower mitochondrial gene expression (Extended Data Fig. 1d), suggesting altered mitochondrial metabolism. Annotations were validated by plotting the expression of meningeal, white matter and layer-specific gray matter genes (Extended Data Fig. 1e).

We used a pseudobulk method (DESeq2) to identify differentially expressed genes (DEGs) per region. Deeper cortical layers showed the most DEGs in nAD versus NND controls, while superficial layers were mostly affected in iAD versus nAD controls (Fig. 1e). Cortical layer III exhibited many DEGs in both iAD versus nAD and nAD versus NND comparisons. This high level of transcriptomic dysregulation led us to further examine this cortical layer. Nearly all cortical layer III DEGs were unique to iAD or nAD compared to their controls, with only 7.1% shared (Fig. 1f). These results indicate transcriptomic alterations in superficial layers of the actively immunized AD cortex.

Notably, the triggering receptor expressed on myeloid cells 2 (*TREM2*) and apolipoprotein E (*APOE*) were among the genes

upregulated in cortical layer III of the iAD cortex compared to nAD controls (Fig. 1g,h). Both genes are established AD risk factors^{19–22} and are associated with the microglial response to A β ^{23–26}. Additional upregulated cortical layer III genes in iAD versus nAD included alpha-2-macroglobulin (*A2M*) and caveolae-associated protein 1 (*CAVIN1*), involved in inflammation and lysosomal function. Down-regulated genes in iAD versus nAD included those encoding heat shock proteins (HSPs), such as heat shock protein family A (*Hsp70*) member 1A (*HSPA1A*) and heat shock protein family H (*Hsp110*) member 1 (*HSPH1*; Fig. 1g,h). HSPs, involved in protein folding²⁷ and cellular stress^{27,28}, were increased in nAD compared to NND controls (Fig. 1h and Extended Data Fig. 1f). Examination of the most divergent DEGs between iAD versus nAD and nAD versus NND showed that HSP genes were down-regulated after immunization but showed the opposite direction in nAD compared to NND (Extended Data Fig. 1g). Conversely, synaptic plasticity-associated genes, such as semaphorin 3G (*SEMA3G*) and Hes family BHLH transcription factor 5 (*HES5*) were upregulated in iAD brains. These findings show transcriptomic alterations in cortical layer III after immunization, including decreased protein folding and stress genes and increased microglial response genes like *APOE* and *TREM2*.

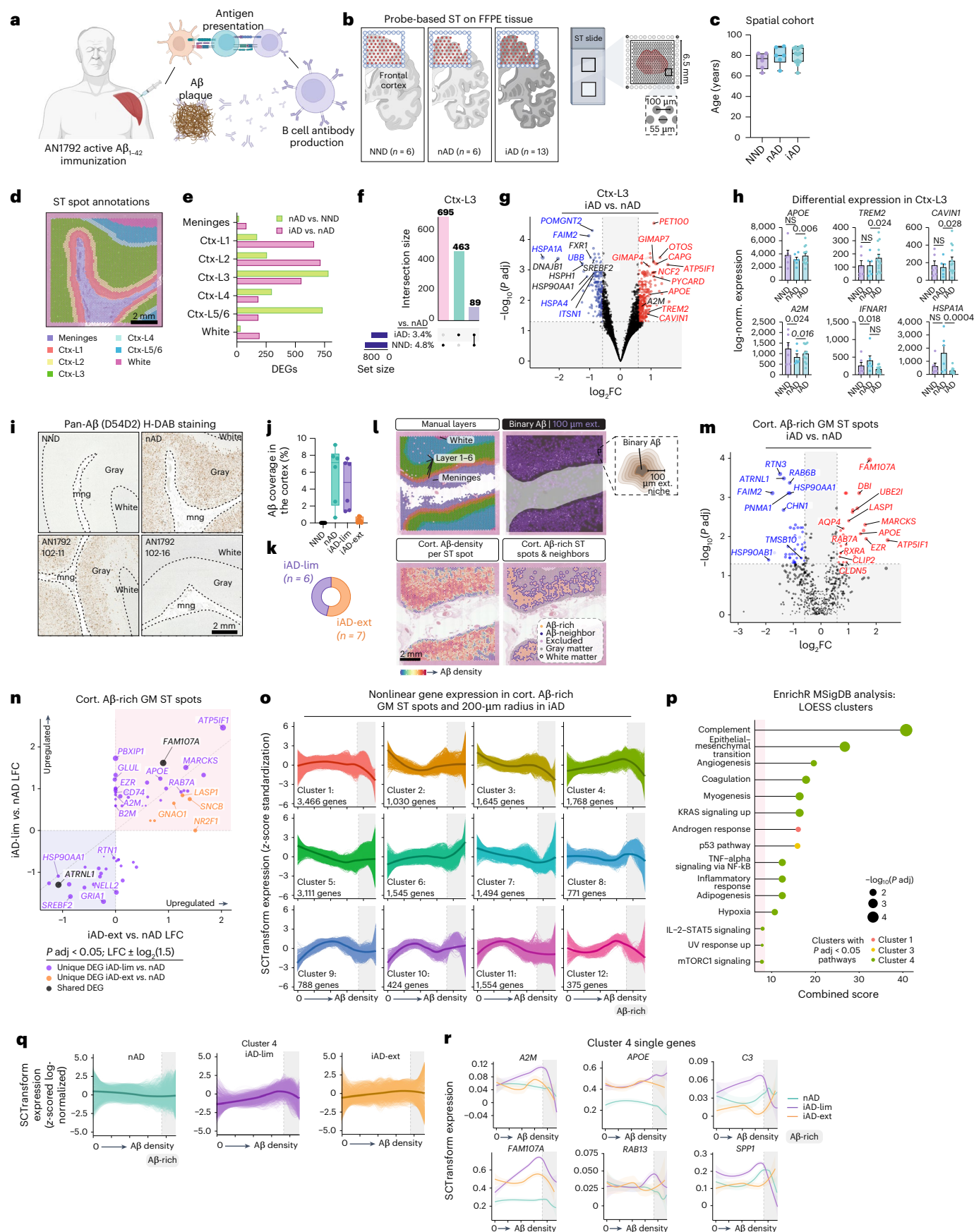
We previously demonstrated A β clearance in a subset of AN1792 patients^{3–5,16}. To investigate mechanisms driving varying degrees of A β clearance in AN1792 patients, we quantified A β pathology on sequential slides of ST tissue using immunohistochemistry (IHC; Fig. 1i and Extended Data Fig. 1h). A β clearance was most prominent in the superficial cortical layers (Extended Data Fig. 1i), consistent with our previous findings⁴. The iAD cohort was categorized into those with limited (iAD-lim, $N = 6$) and extensive (iAD-ext, $N = 7$) A β clearance based on amounts of residual A β coverage (Fig. 1j,k). Phosphorylated tau (pTau) was quantified using AT8 load in gray matter across these groups, revealing no significant differences (Extended Data Fig. 1j,k). This dovetails with our prior results showing tau pathology persisted in A β -cleared cortical areas¹⁶.

To capture transcriptomic alterations around A β deposits, we overlaid A β IHC images from consecutive slides (5–10 μ m apart) with ST data and extended the A β signal by 100 μ m with decreasing intensity every 20 μ m (Fig. 1l). This enabled direct examination of the A β niche and associated genes. Vascular A β -rich ST spots were excluded from analyses. Differential expression analysis of A β -rich ST spots in gray matter using model-based analysis of single-cell transcriptomics (MAST)²⁹ revealed increased expression of *APOE* and myristoylated alanine-rich C-kinase substrate (*MARCKS*; Fig. 1m) in iAD A β niches. *MARCKS* is expressed in activated microglia that surround A β plaques³⁰.

Fig. 1 | Active A β immunization sustains inflammation at the A β niche.

a, AN1792 active A β immunization. Created with BioRender.com. **b**, ST method and group sizes of NND, nAD and iAD FCX tissues. Created with BioRender.com. **c**, Study demographics indicating age of each patient. **d**, Manually annotated ST spots in the FCX. **e**, Number of DEGs for each comparison per manually annotated area. **f**, UpSet plot showing unique and shared DEGs across group comparisons in cortical layer III. **g**, DEGs in cortical layer III (iAD versus nAD). Red and blue DEGs are uniquely identified in the iAD versus nAD comparison and are not observed as DEGs in the nAD versus NND comparison. **h**, Pseudobulked expression for various genes in microglia-enriched gray matter ST spots. Error bars indicate the s.e.m. *P* values are from DESeq2. **i**, Representative pan-A β H-DAB stains for each group. **j**, Quantification of cortical A β coverage per group. **k**, Numbers of iAD-lim and iAD-ext patients among AN1792 actively immunized patients. **l**, Method of processing of A β IHC images. The binary A β signal was extended by 100 μ m beyond its actual size, with a gradual decrease in signal intensity every 20 μ m, allowing for detection of genes associated with A β density. **m**, DEGs from A β -rich gray matter ST spots (iAD versus nAD). **n**, LFC plots for A β -rich ST spots in gray matter (iAD-lim versus nAD; iAD-ext versus nAD). **o**, LOESS plots showing clusters of nonlinear gene expression patterns relative to A β density in iAD. **p**, Pathway enrichment analysis of genes in nonlinear expression clusters associated with A β density in iAD. **q**, LOESS plot of cluster 4 predictions in nAD, iAD-lim and iAD-ext

relative to A β density. **r**, LOESS plots of select genes in LOESS cluster 4. Dark line indicating the LOESS predicted expression, and light shading represents standard error of the estimated values. **c,j**, Box plots are bounded by the 25th and 75th percentiles, the center line shows the median, and whiskers show the data range. **o,q**, LOESS plots with the dark line represent the mean LOESS predicted expression per group per cluster, and single lines indicate LOESS predicted gene expression per group per cluster. **c,e–h,j,k**, NND = 6; nAD = 6; iAD = 13; iAD-lim = 6; iAD-ext = 7. **m,n**, nAD = 4; iAD = 10; iAD-lim = 6; iAD-ext = 4. **o–r**, nAD = 4; iAD = 12; iAD-lim = 6; iAD-ext = 6. DESeq2 (e–h) or MAST (m and n) was used to compare expression levels. For DESeq2, covariates included sex, age, average genes detected and genomic DNA (gDNA) percentage. In MAST, manually annotated region or cortical layer, sex, age, cellular detection rate (CDR) and gDNA percentage were included as covariates, with sample ID as a random effect. All *P* values were false discovery rate (FDR)-adjusted using Benjamini–Hochberg correction. A2M, alpha-2-macroglobulin; APOE, apolipoprotein E; CAVIN1, caveolae-associated protein 1; Ctx, cortex; FFPE, formalin-fixed paraffin-embedded; GM, gray matter; HSPA1A, heat shock protein family A member 1A; H-DAB, hematoxylin-3,3'-diaminobenzidine; IFNARI, interferon alpha and beta receptor subunit 1; LFC, log fold change; MSigDB, Molecular Signatures Database; *P*adj, adjusted *P* value. NS, not significant.



The most upregulated gene at the A β niche was family with sequence similarity 107 member A (*FAM107A*), a stress-responsive actin-bundling factor influencing synaptic efficiency and cognition³¹.

Comparison of the A β niche between iAD-lim and iAD-ext brains revealed upregulation of inflammatory genes like beta-2-microglobulin (*B2M*), *A2M*, *CD74* molecule (*CD74*), *APOE* and *MARCKS* in iAD-lim but not iAD-ext brains (Fig. 1n). Pathway analyses revealed enrichment of interferon alpha response and interleukin-2 (IL-2)-STAT5 signaling in the iAD-lim A β niche (Extended Data Fig. 1l). Collectively, genes altered in A β -rich ST spots show an inflammatory signature within the A β niche of iAD-lim versus iAD-ext.

We visualized nonlinear relationships between gene expression and A β density in A β -rich ST spots (200- μ m radius) using locally estimated scatterplot smoothing (LOESS; Extended Data Fig. 1m,n). Hierarchical clustering delineated distinct expression patterns with increasing A β density within the iAD group (Fig. 1o). Pathway analysis of gene clusters revealed that cluster 4, peaking in A β -rich ST spots, was enriched for immune-related pathways, including complement signaling, inflammatory response and IL-2-STAT5 signaling (Fig. 1p). Cluster 4 genes showed the highest upregulation in iAD-lim A β niches, a lesser increase in iAD-ext and no upregulation in nAD (Fig. 1q). This cluster contained many immune-associated genes, including *A2M*, *APOE*, complement C3 (*C3*), member RAS oncogene family (*RAB13*) and secreted phosphoprotein 1 (*SPPI*; Fig. 1r). Together, these findings reveal sustained inflammation at the A β niche in AN1792-immunized brains with limited A β clearance, marked by IL-2-STAT5 and complement signaling, and upregulation of inflammatory response genes in AD.

Microglial phenotypes define varying degrees of A β clearance

Because ST spots encompass 1–10 cells each, we aimed to resolve their cellular composition using Cell2Location (C2L)³², which integrates ST data with single-nucleus RNA sequencing (snRNA-seq). We constructed a reference atlas from a snRNA-seq dataset of 424 dorsolateral prefrontal cortex (DLPFC) tissues from AD and NND controls^{33,34}, downsampling to 34,695 cells for near-equal cell-type representation (Fig. 2a and Extended Data Fig. 2a). C2L analysis mapped cell types to expected spatial locations (Fig. 2b and Extended Data Fig. 2b). In the gray matter after AN1792 immunization, excluding layer I due to unreliable cell mapping, we observed increased relative numbers of astrocytes and reduced layer 2/3 (L2/3) excitatory neurons (ENs), although these changes were not statistically significant. Microglia were predicted to be most abundant in the iAD-lim cortex (Extended Data Fig. 2c).

We then annotated the most highly enriched ST spots for specific cell types within their expected spatial regions (Fig. 2c). Comparing iAD to nAD gene expression in cell-type-enriched ST spots showed most DEGs in L2/3 EN-enriched ST spots, followed by microglia and astrocytes (Fig. 2d and Extended Data Fig. 2d). Conversely, nAD samples

showed DEGs predominantly in layer 4/5 (L4/5) ENs, interneurons and L2/3 ENs when compared to NND (Fig. 2d and Extended Data Fig. 2e). Microglia-enriched ST spots in iAD versus nAD showed the upregulation of *APOE*, *TREM2*, *A2M*, *RAB13*, *FAM107A* and other amyloid-response genes such as lysosomal-associated membrane protein 1 (*LAMP1*), *CD163* molecule (*CD163*), PYD and CARD domain containing (*PYCARD*), integrin subunit alpha X (*ITGAX*) and apolipoprotein C1 (*APOC1*), while HSP genes were downregulated (Fig. 2e). Top divergent DEGs between iAD versus nAD and nAD versus NND (for example, *Dnaj* heat shock protein family (*Hsp40*) member A1 (*DNAJA1*) and *Fas* apoptotic inhibitory molecule 2 (*FAIM2*)) indicated reduced cellular stress and disrupted apoptosis after AN1792 (Fig. 2f).

Differential expression analysis of microglia-enriched ST spots revealed more DEGs in iAD-ext than in iAD-lim compared to nAD, indicating a more distinct microglial state with extensive A β clearance (Fig. 2g and Extended Data Fig. 2f,g). Unique iAD-ext upregulated genes included *APOE*, *MARCKS* and fibroblast growth factor receptor 3 (*FGFR3*; Fig. 2h). FGFR3 serves as a receptor for fibroblast growth factor 2 (FGF2), which neurons release in response to oligomeric A β -induced damage. This interaction promotes microglial migration and debris phagocytosis, aiding in neuroprotection³⁵. In iAD-lim, we found upregulation of previously mentioned *TREM2*, *A2M* and *LAMP1*, as well as transmembrane immune signaling adaptor TYROBP (*TYROBP*), which links *TREM2* to *APOE* transcription in microglia³⁶. Shared upregulated genes included *PYCARD* and Toll-like receptor 7 (*TLR7*; Fig. 2h and Extended Data Fig. 2f,g), while non-shared genes showed similar trends without significance in both groups (Fig. 2i). *PYCARD* activates the inflammasome, forming apoptosis-associated speck-like protein containing a CARD (ASC) specks that can cross-seed A β pathology³⁷. Localization of proteins TMS1/ASC (encoded by *PYCARD*), *A2M* and *APOE* was confirmed in IBA1 $^+$ microglia around A β plaques in the AN1792-immunized FCX (Fig. 2j-l).

Most divergent genes in microglia-enriched ST spots between A β clearance groups were leukocyte-specific protein 1 (*LSP1*) and GTPase of immunity-associated protein (*GIMAP*) genes in iAD-lim and *FGFR3* and *HSPA1A* in iAD-ext (Extended Data Fig. 2h). *LSP1* localizes to nascent phagocytic cups during Fc γ -receptor-mediated phagocytosis³⁸. Pathway analysis revealed increased IL-2-STAT5 signaling in both groups, with iAD-ext uniquely upregulating oxidative phosphorylation and adipogenesis, while iAD-lim showed downregulation of complement and unfolded protein response pathways (Fig. 2m).

We next examined genes shared between iAD-ext versus nAD and NND versus nAD in microglia-enriched regions to determine if transcriptomic changes in iAD-ext brains reflect a return to homeostasis similar to NND. Shared upregulated genes included *FGFR3*, cold-inducible RNA-binding protein (*CIRBP*) and sorbin and SH3 domain containing 3 (*SORBS3*), while downregulated genes included

Fig. 2 | Microglial phenotypes define varying degrees of A β clearance.

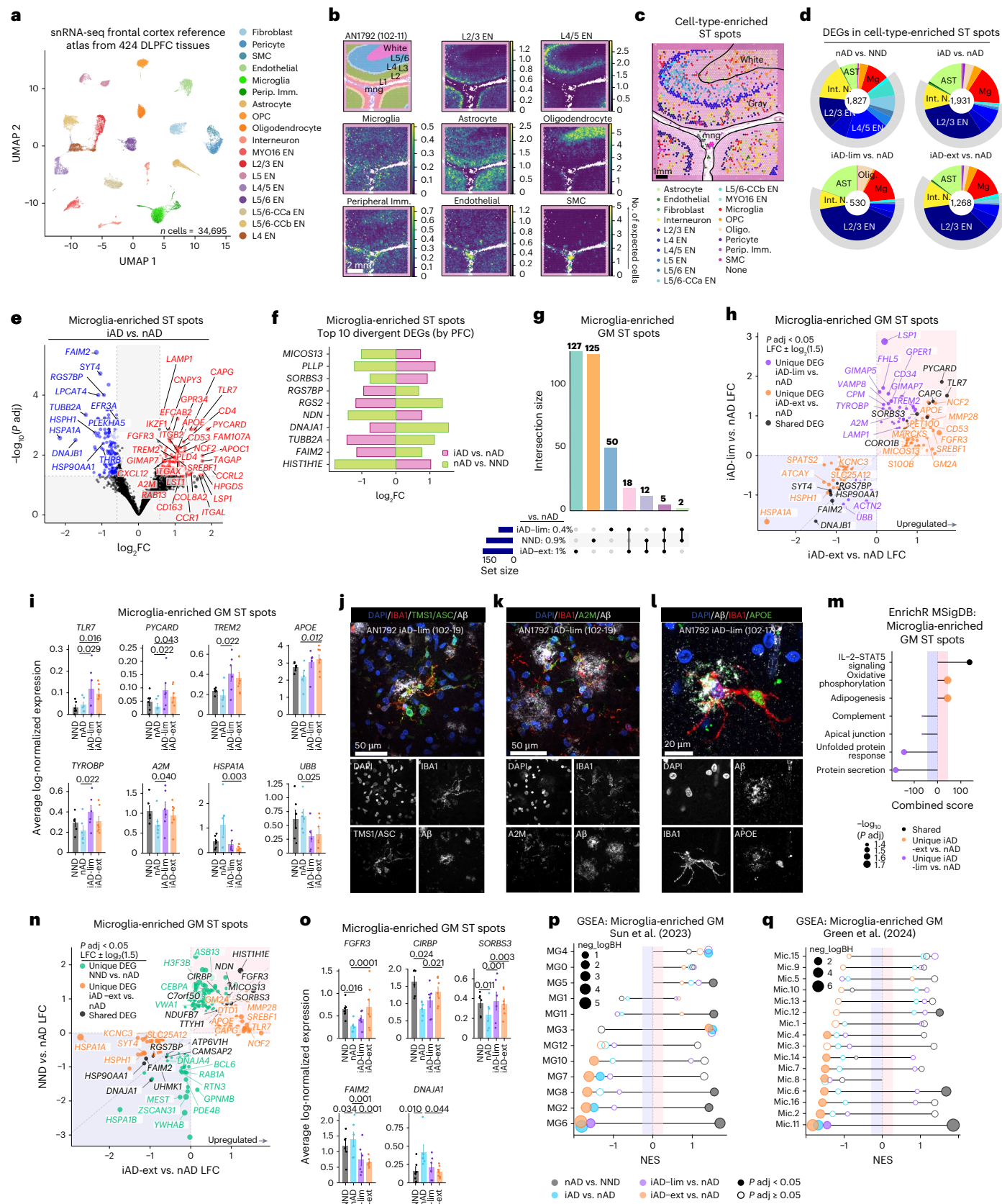
a, Reference atlas UMAP from DLPFC snRNA-seq data^{33,34}. **b**, Spatial plots showing abundance of deconvoluted cell types. **c**, Spatial plots highlighting enriched ST spots for deconvoluted cell types. **d**, Percentages of DEGs expressed in enriched ST spots per cell type: nAD versus NND, iAD versus nAD, iAD-lim versus nAD and iAD-ext versus nAD. The number in the center of each pie chart represents the total number of DEGs. **e**, DEGs from microglia-enriched ST spots (iAD versus nAD). **f**, Top ten divergent DEGs in microglia-enriched ST spots based on PFC, comparing iAD versus nAD and nAD versus NND. **g**, UpSet plot showing unique and shared DEGs in microglia-enriched ST spots in gray matter across groups compared to nAD. **h**, LFC plots for microglia-enriched ST spots in gray matter (iAD-lim versus nAD; iAD-ext versus nAD). **i**, Pseudobulked expression for various genes in microglia-enriched ST gray matter spots. Error bars show the s.e.m. *P* values are from DESeq2. **j–l**, Confocal images showing TMS1/ASC $^+$ IBA1 $^+$ myeloid cells (j), A2M $^+$ IBA1 $^+$ myeloid cells (k) and APOE $^+$ IBA1 $^+$ myeloid cells (l) around A β deposits in the FCX of iAD. **m**, Pathway enrichment analysis of unique and shared DEGs in microglia-enriched gray matter ST spots (iAD-lim versus nAD; iAD-ext versus nAD). **n**, LFC plots for microglia-enriched gray matter ST spots (NND

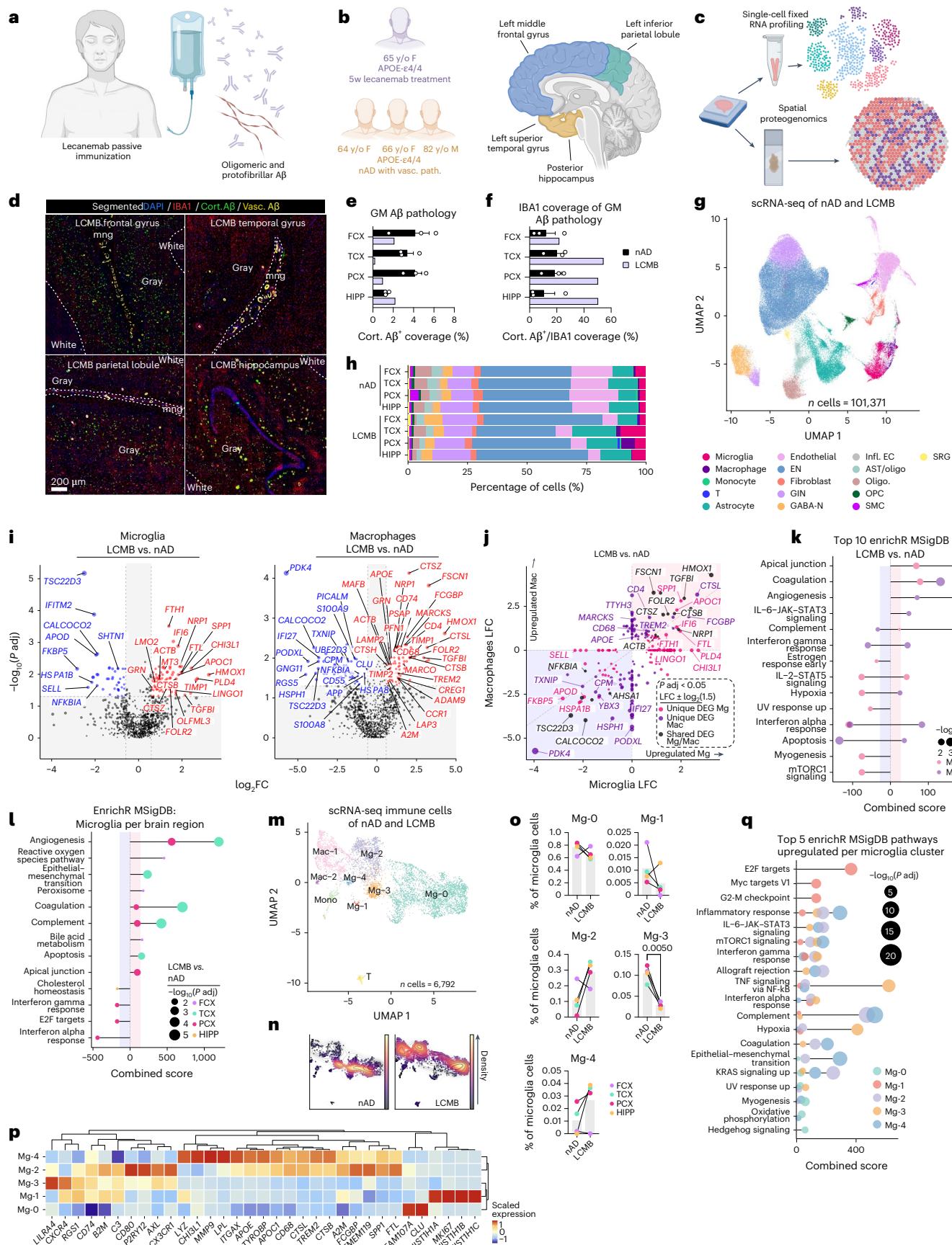
versus nAD; iAD-ext versus nAD). **o**, Pseudobulked expression for various genes in microglia-enriched ST spots in gray matter. Error bars show the s.e.m. *P* values are from DESeq2. **p–q**, Pathway enrichment analysis of predefined microglial states from p⁴¹ and q³⁴, using genes ranked by PFC in iAD-lim versus nAD and iAD-ext versus nAD. **i, o**, Bar plots display means \pm s.e.m. **d–i, m–q**, NND = 6; nAD = 6; iAD = 13; iAD-lim = 6, iAD-ext = 7. DESeq2 was used to compare expression levels, with sex, age, average genes detected and gDNA percentage included as covariates (**d–i** and **n–o**). All *P* values were FDR adjusted using Benjamini-Hochberg. Ast, astrocyte; CCa, cortico-cortical cluster a; CCb, cortico-cortical cluster b; CIRBP, cold-inducible RNA-binding protein; FAIM2, Fas apoptotic inhibitory molecule 2; FGFR3, fibroblast growth factor receptor 3; GSEA, gene-set enrichment analysis; IBA1, ionized calcium-binding adapter molecule 1; Int. N., interneuron; L, layer; Mg, microglia; NES, normalized enrichment score; OPC, oligodendrocyte precursor cell; Perip. Imm., peripheral immune cells; PYCARD, PYD and CARD domain containing; SMC, smooth muscle cell; SORBS3, sorbin and SH3 domain containing 3; TLR7, Toll-like receptor 7; TYROBP, TYRO protein tyrosine kinase-binding protein; UBB, ubiquitin B; UMAP, uniform manifold approximation and projection.

FAIM2, *DNAJA1* and heat shock protein 90 alpha family class A member 1 (*HSP90AA1*; Fig. 2n,o). *CIRBP* is a stress-responsive gene that modulates inflammation³⁹ and ameliorates neuronal amyloid toxicity via antioxidative and antiapoptotic pathways⁴⁰. These findings suggest

that some DEGs in microglia-enriched ST spots of iAD-ext brains reflect a shift in microglial gene expression toward an NND control profile.

To investigate microglial function after AN1792 immunization, we compared microglia-enriched ST spot signatures of iAD brains to





published human AD microglial states^{34,41}. Here, iAD brains after AN1792 immunotherapy showed reduced stress-responsive microglia (MG6), inflammatory states (MG2, MG8, MG10) and glycolytic microglia (MG7),

and increased ribosome biogenesis microglia (MG3; Fig. 2p). Notably, MG3 microglia exhibit strong enrichment of disease-associated microglia (DAM) signature genes⁴¹. In contrast, inflammatory and

Fig. 3 | Passive Aβ immunization induces distinct microglial states.

a, Lecanemab binds oligomeric and protofibrillar Aβ to promote Aβ clearance from the brain. Created with BioRender.com. **b**, Study participants included a 65-year-old female patient with AD who was treated with lecanemab and three matched nAD controls. Tissues analyzed included cortical areas and HIPP. Created with BioRender.com. **c**, Tissues were analyzed by scRNA-seq and spatial proteogenomics. Created with BioRender.com. **d**, Confocal images showing segmented Aβ burden and microgliosis in regions of the lecanemab-treated patient brain. **e**, Percentage of cortical Aβ coverage in brain regions from the lecanemab case and nAD controls. **f**, Percentage of cortical Aβ covered by IBA1. **g**, UMAP showing annotated cell types. **h**, Percentages of each cell type for each brain region between nAD controls and lecanemab case. **i**, DEGs in microglia and macrophages comparing lecanemab to nAD. **j**, LFC plots comparing DEGs in microglia and macrophages (lecanemab versus nAD). **k**, Top ten pathway enrichment analysis of DEGs in microglia and macrophages (lecanemab versus nAD). **l**, Pathway enrichment analysis of DEGs in microglia from FCX, TCX, PCX

and HIPP (lecanemab versus nAD). **m**, Clustering of microglia from scRNA-seq of the lecanemab case and nAD controls. **n**, UMAP density plots showing microglial cluster distribution for the lecanemab case and nAD controls. **o**, Percentages of microglial clusters in the lecanemab case versus nAD controls. Normality tests dictated if *P* values were calculated using a two-tailed paired *t*-test or Wilcoxon test. **p**, Marker genes for each microglial cluster. **q**, Top five upregulated pathways using marker genes defining the microglial states. **e,f,o**, Bar plots display means ± s.e.m. **o**, Bar plots display means. **e,f,o**, Statistical tests, guided by Shapiro–Wilk and *F* tests, included *t*-tests, Mann–Whitney tests (**e** and **f**) and paired *t*-tests (**o**). **e–q**, nAD = 3; LCMB = 1. **i,j**, MAST was used to compare expression levels, with brain region and CDR as covariates and brain region and sample ID included as a random effect. **i–l,q**, *P* values were FDR adjusted using Benjamini–Hochberg. Cort., cortical; GABA-N, GABAergic neuron; GIN, GABAergic interneuron; Infl. ECs, inflamed endothelial cells; LCMB, lecanemab; Mac, macrophages; mng, meninges; Oligo, oligodendrocyte; SRG, stress-responsive glia; Vasc, vascular.

stress-responsive microglia states were increased in nAD versus NND. Using separate microglial classifications³⁴ showed a reduction in stress-responsive microglia (Mic.11), surveilling microglia (Mic.2, Mic.4), reactive microglia (Mic.6–Mic.8), interferon-responsive microglia (Mic.14) and serpin family E member 1 (*SERPINE1*)-expressing microglia (Mic.16) after immunization (Fig. 2g).

Overall, active Aβ immunization reduces stress-responsive microglia irrespective of residual Aβ levels. Yet, microglia in iAD-ext shifted from glycolysis to oxidative phosphorylation, while iAD-lim showed decreased complement and unfolded protein responses with upregulated phagocytosis genes. These findings suggest that effective Aβ clearance relies on balanced microglial metabolic states that also protect against Aβ neurotoxicity.

Passive Aβ immunization induces distinct microglial states

Intrigued by the microglial response to Aβ in actively immunized AD brains, we extended our investigation to examine immune responses to passive lecanemab immunization (Fig. 3a). We analyzed a unique case of a patient with AD who received three lecanemab infusions over 5 weeks, shortly before passing away from intracerebral hemorrhages^{17,18}. Our postmortem analysis revealed histiocytic vasculitis in CAA-affected vessels, with vascular Aβ fragmentation and phagocytosis across the cortex, alongside a ‘high’ burden of AD pathology per National Institute on Aging and Alzheimer’s Association (NIA-AA) guidelines^{17,18}. Notably, parenchymal Aβ plaque phagocytosis was also observed¹⁸. We compared this patient to three *APOE*ε4/ε4-matched controls with high AD pathology and vascular AD pathology without anti-Aβ treatment (Fig. 3b and Extended Data Table 2). Cortical tissues studied were from the left middle FCX, superior temporal cortex (TCX) and inferior parietal lobule (PCX), as well as the posterior hippocampus (HIPP). These regions were selected for their varying levels of Aβ clearance in this patient brain¹⁸. We used scRNA-seq and spatial proteogenomics to identify cell-type-specific immune responses to passive Aβ immunization in these regions (Fig. 3c).

Tissue sections were stained for IBA1 and pan-Aβ. Using manual annotation and machine learning, we differentiated cortical and vascular Aβ pathology (Fig. 3d and Extended Data Fig. 3a). Gray matter Aβ quantification showed reduced cortical Aβ in the TCX and PCX of the lecanemab case compared to controls (Fig. 3e). Moreover, a higher fraction of cortical Aβ (~44%) was covered by IBA1⁺ cells in the lecanemab case versus ~15% in controls (Fig. 3f). These data indicate regional variability in Aβ clearance by myeloid cells.

To further explore immune responses to Aβ following passive immunization, we performed scRNA-seq on cells isolated from each brain region, and used SoupX⁴² to minimize ambient RNA contamination (Extended Data Fig. 3b). We assessed quality-control metrics (Extended Data Fig. 3c,d), integrated cells from all tissues (Extended Data Fig. 3e) and annotated cell clusters using their highly expressed genes (Fig. 3g and Extended Data Fig. 3f). The lecanemab case showed a relative increase in GABAergic interneurons and a decrease in endothelial cells, fibroblasts and smooth muscle cells (Fig. 3h and Extended Data Fig. 3g). T cells were enriched in all regions except HIPP, monocytes/macrophages in PCX and TCX, and microglia in TCX, PCX and HIPP (Fig. 3h and Extended Data Fig. 3g).

Differential expression analysis of microglia and macrophages revealed upregulated genes linked to microglial activation (*SPP1* and chitinase 3 like 1 (*CHI3L1*)), lysosomal function (cathepsin B (*CTSB*), granulin (*GRN*)), and interferon response (interferon alpha inducible protein 6 (*IFI6*)) in the lecanemab case (Fig. 3i). Additional upregulated genes included those linked to iron storage (ferritin heavy chain 1 (*FTH1*), ferritin light chain (*FTL*)) and lipid metabolism (*APOC1*; Fig. 3i). *SPP1* and *APOC1* were the most upregulated genes unique to microglia (Fig. 3j). *SPP1* is expressed by activated-response microglia⁴³ and contributes to tissue repair⁴⁴. We confirmed expression of *SPP1* and *APOC1* proteins in plaque-associated microglia within the HIPP following lecanemab treatment (Extended Data Fig. 3h,i). Macrophage-specific upregulated genes included *TREM2*, *APOE* and the phagocytosis-associated gene cluster of differentiation 68 (CD68)

Fig. 4 | Spatial proteogenomics links the Aβ niche to microglial states.

a, Proteogenomics allowed for the simultaneous profiling of RNA and protein from lecanemab-treated and nAD controls. Created with BioRender.com. **b**, Manual annotations of brain regions analyzed. **c**, Representative images showing distinction of segmented cortical and vascular Aβ in brain regions from the lecanemab case. **d**, Number of DEGs for each comparison across manually annotated areas. **e**, DEGs from Aβ-rich gray matter ST spots (lecanemab versus nAD) in FCX, TCX, PCX and HIPP. **f**, Top ten pathway enrichment analysis of DEGs in Aβ-rich gray matter ST spots for each brain region (lecanemab versus nAD). **g**, DEPs associated with cortical Aβ ST spots from each brain region (lecanemab versus CAA control), with pink indicating shared DEGs, green indicating no shared DEGs and black indicating low expression levels not meeting DEG criteria. **h**, Confocal images showing CD68⁺IBA1⁺ myeloid cells surrounding Aβ deposits in

the HIPP of the lecanemab-treated patient. **i**, LOESS plot of cluster 3 predictions in nAD (left) and lecanemab (right) relative to Aβ density. Dark line represents the mean LOESS predicted expression per group per cluster and single lines indicate LOESS predicted gene expression per group per cluster. **j**, LOESS plots of selected genes in LOESS cluster 3. Dark line indicates the LOESS predicted expression and light shading represents standard error of the estimated values. **d–g,i,j**, nAD = 3; LCMB = 1. DESeq2 (**d**), MAST (**e**) or FindMarkers with a negative binomial model (**g**) was used to compare expression levels. For DESeq2, covariates included brain region, average genes detected and gDNA percentage. In the MAST model, manually annotated region or cortical layer, gDNA percentage and CDR were included as covariates, with brain region and sample ID as a random effect. For FindMarkers, covariates included manually annotated region or cortical layer and CDR. All *P* values were FDR adjusted using Benjamini–Hochberg.

molecule (*CD68*; Fig. 3j). Both cell types exhibited decreased HSP gene expression, while heme oxygenase 1 (*HMOX1*), the most upregulated gene shared between them, reflected an immune response to hemorrhages in the lecanemab case.

To study microglia and macrophage functions after immunization, we performed enrichment analysis. Pathways regulating vascular functions such as apical junctions, coagulation and angiogenesis were upregulated in macrophages and microglia in the lecanemab case

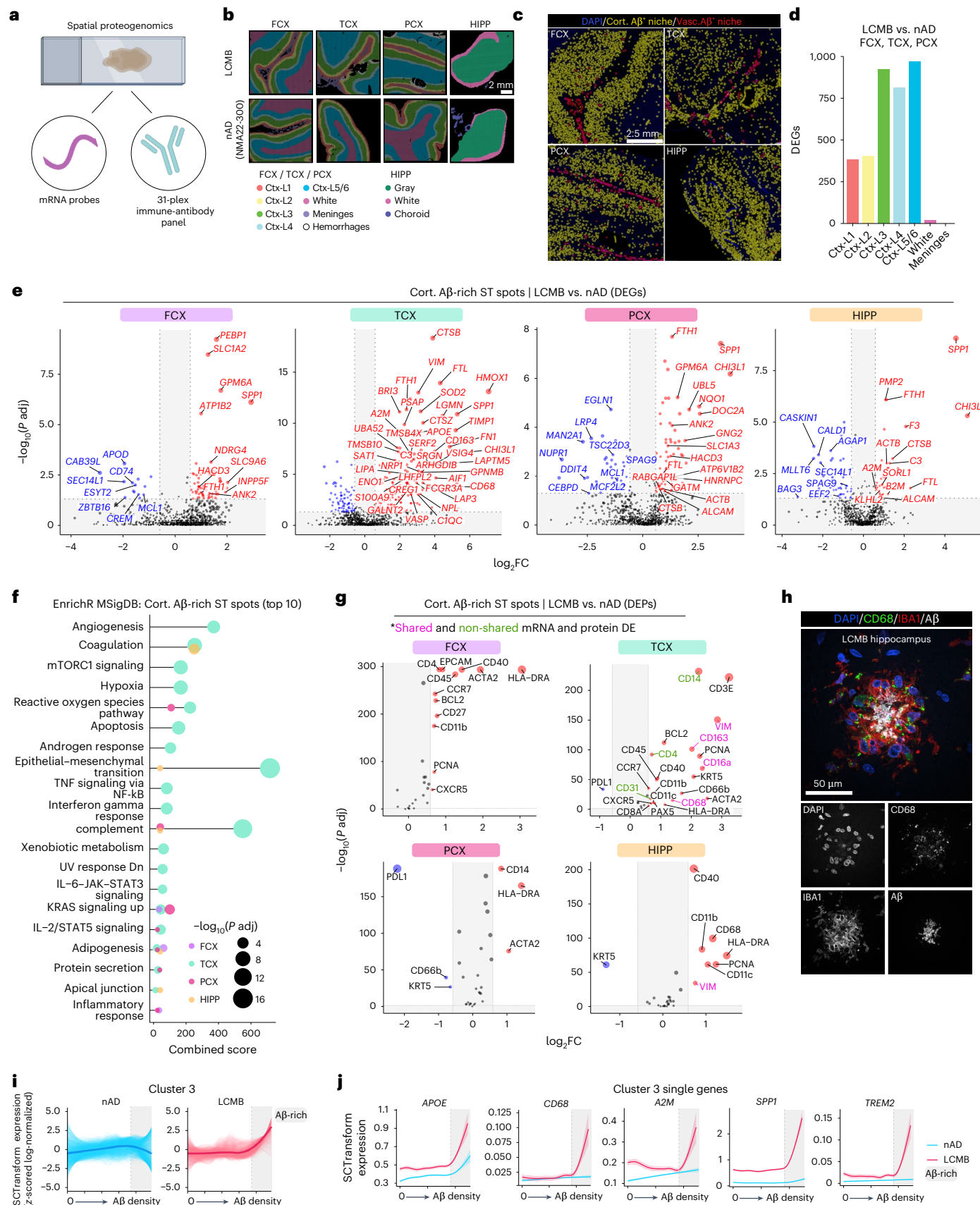


(Fig. 3k). Additionally, we found dysregulated complement signaling in macrophages and increased complement signaling in microglia (Fig. 3k). We also observed dysregulated IL-2–STAT5 signaling in microglia, with both downregulated and upregulated DEGs associated with this pathway (Fig. 3k). These data highlight distinct alterations to the brain myeloid compartment following passive A β immunization.

Notably, microglial transcriptomic signatures in the lecanemab case varied by brain region (Extended Data Fig. 3j). Most changes in microglial gene expression were observed in the TCX and PCX, the two regions with the most A β clearance. Microglia from these regions exhibited increased expression of genes involved in complement signaling (*C3*), lysosomal function and protein degradation (for example, cathepsin genes), iron storage and regulation (*FTH1*, *FTL*) and *SPP1* (Extended Data Fig. 3j). Regional DEGs were associated with various signaling pathways. In the FCX, DEGs indicated increased reactive oxygen species signaling (Fig. 3l). The TCX and PCX showed increased complement signaling, while the PCX also exhibited decreased interferon responses, among other changes (Fig. 3l). The HIPP demonstrated decreased cholesterol homeostasis (Fig. 3l). Additionally, microglial DEGs were linked to vascular pathways (for example, angiogenesis and coagulation), but this association was present only in the TCX and PCX, areas with extensive A β clearance (Fig. 3l). Thus, distinct microglial phenotypes may underlie the variability in A β clearance between brain regions of the lecanemab case.

Microglial states⁴¹ were also altered, with reduced inflammatory MG8 microglia and increased ribosomal biogenesis MG3 microglia across brain regions in the lecanemab case (Extended Data Fig. 3k). In the FCX, where IBA1-A β recruitment was low, reductions were seen in inflammatory (MG2, MG8, MG10), phagocytic (MG5), stress-signature (MG6) and glycolytic (MG7) microglia. Conversely, inflammatory MG10 microglia increased in the PCX where IBA1-A β recruitment and A β clearance were high. Separate microglial classifications³⁴ showed a similar pattern with several microglial states downregulated in the FCX, that were upregulated in the TCX, PCX and HIPP regions (Extended Data Fig. 3l). These findings reveal a reduction in inflammatory MG8 microglia and an increase in ribosome biogenesis and DAM-expressing MG3 microglia across all brain regions after lecanemab immunization, similar to AN1792. Notably, the FCX displayed a distinct microglial profile compared to other brain regions.

Immune cell sub-clustering identified two microglial states, Mg-2 and Mg-4, that were enriched in lecanemab-treated brain regions with

most IBA1-A β recruitment and A β clearance (Fig. 3m–o and Extended Data Fig. 3m–o). Mg-2 exhibited a mixed DAM and homeostatic profile, expressing *TREM2*, *APOE* and homeostatic markers, along with high levels of AXL receptor tyrosine kinase (*AXL*), *C3*, *CD74* and *SPP1* (Fig. 3o,p). Mg-4 displayed a classic DAM signature, with elevated *ITGAX*, lipoprotein lipase (*LPL*), matrix metallopeptidase 9 (*MMP9*), *CHI3L1* and *SPP1* (Fig. 3o,p). Both clusters showed enhanced complement pathway signaling (Fig. 3q).

In summary, we identified upregulated genes (for example, *SPP1* and *APOC1*) in microglia after lecanemab treatment. Additionally, we observed two distinct microglial phenotypes in brain regions with A β clearance, both expressing *APOE* and *TREM2*, and showing increased complement signaling. These findings demonstrate that passive A β immunization triggers specific microglial adaptations associated with A β clearance.

Spatial proteogenomics links the A β niche to microglial states

Having established microglial responses to lecanemab using single-cell analysis, we next used spatial proteogenomics on adjacent tissue sections to investigate the immune response at the A β niche (Fig. 4a). An 11 × 11-mm ST capture area (14,336 spots) was analyzed, with ST spots annotated using DAPI staining to delineate meninges, cortical layers and white matter, and to exclude hemorrhagic regions (Fig. 4b and Extended Data Fig. 4a). Quality-control metrics revealed variability in the number of expressed genes across nAD brains (Extended Data Fig. 4b) and in mitochondrial read percentages (Extended Data Fig. 4c). Yet, regional comparisons showed no significant differences between the nAD group and the lecanemab case. We distinguished cortical and vascular A β , constructed expanded A β niches and defined A β -rich ST spots (Fig. 4c). Consistent with AN1792, we found reduced cortical A β in the superficial layers (I and II; Extended Data Fig. 4d). However, unlike AN1792, differential expression analysis revealed the most DEGs in the deeper cortical layers (III, IV and V/VI; Fig. 4d).

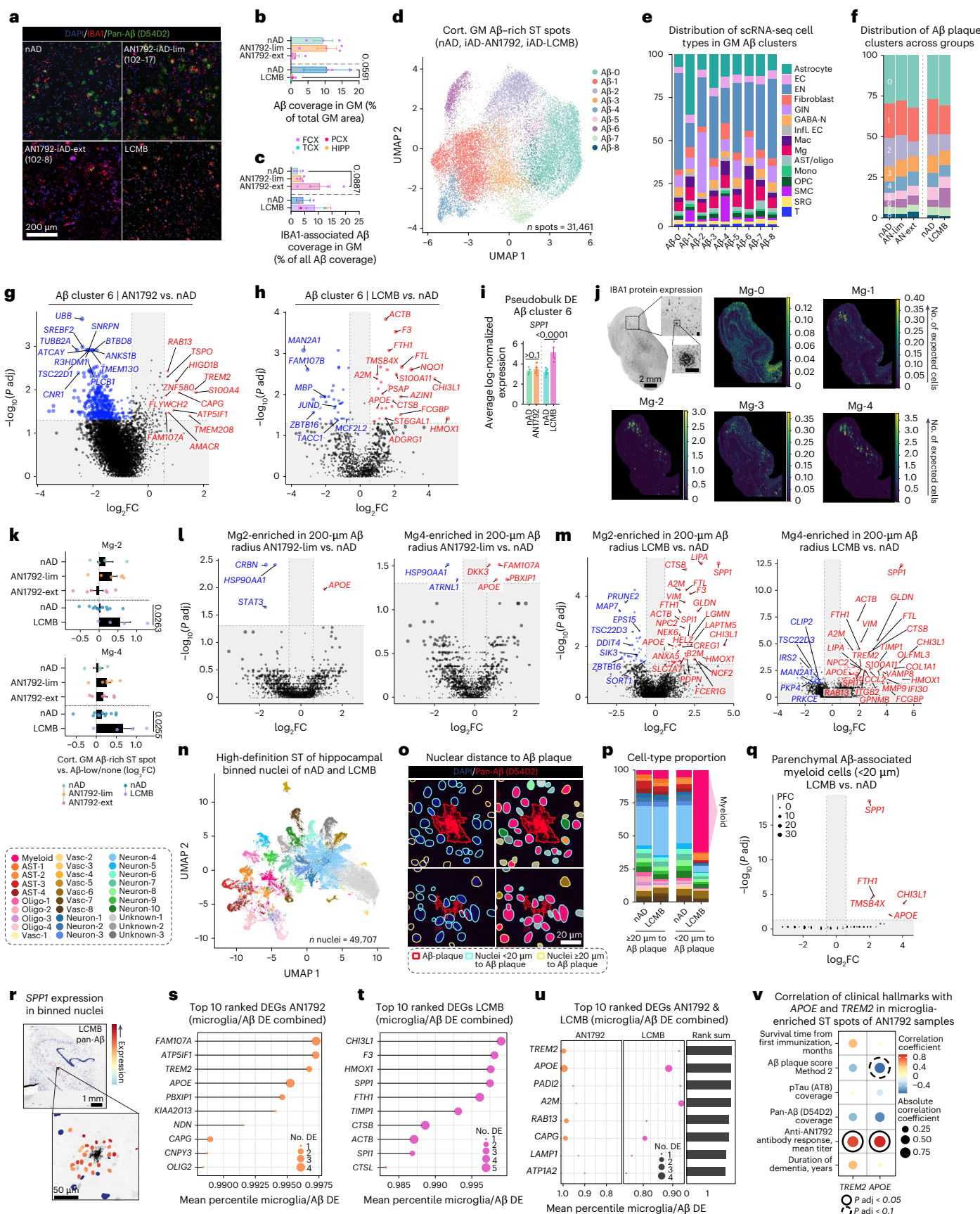
Transcriptomic analysis of cortical A β -positive ST spots showed that residual A β -rich ST spots in regions with the most clearance (TCX and PCX) were the most dysregulated (Extended Data Fig. 4e). In line with the single-cell analysis of microglia in Fig. 3, A β -rich ST spots in the TCX exhibited higher expression of genes related to complement signaling (*C3*, complement C1q C chain (*C1QC*)) and lipid metabolism (*APOE*, lipase A, lysosomal acid type (*LIPA*)); Fig. 4e and Extended Data Fig. 4f). We observed APOE localized to A β plaques surrounded by IBA1⁺

Fig. 5 | Shared microglial response drives A β clearance after immunization. **a**, Confocal images showing pan-A β and IBA1 in FCX brain regions of nAD, AN1792-lim, AN1792-ext and lecanemab-treated patients. **b**, Percentage of cortical A β coverage in cortical and hippocampal regions of AN1792, nAD and the lecanemab case. **c**, Percentage of cortical A β covered by IBA1 in cortical and hippocampal regions of AN1792, nAD and the lecanemab case. **d**, Clustering of A β -rich cortical gray matter spots based on gene expression. **e**, C2L predictions of scRNA-seq cell types in different A β plaque clusters. **f**, Percentages of A β -rich clusters in AN1792, nAD and the lecanemab case. **g,h**, DEGs in A β -rich cluster 6: AN1792 versus nAD (g); lecanemab versus nAD (h). **i**, Pseudobulked *SPP1* expression in A β -rich cluster 6. Error bars indicate the s.e.m. *P* values are from DESeq2. **j**, Spatial plots showing the abundance of deconvoluted scRNA-seq microglia types; scale bar, 100 μ m. **k**, log₂ fold change in predicted abundance of deconvoluted scRNA-seq microglia types in A β -rich ST spots versus the rest in AN1792, nAD and the lecanemab case. **l,m**, DEGs from Mg-2-enriched and Mg-4-enriched A β -associated ST spots: AN1792 versus nAD (l); lecanemab versus nAD (m). **n**, UMAP showing annotated binned nuclei from a high-definition ST assay. **o**, Spatial plots indicating the distance of nuclei to D54D2-stained A β plaques (left) and their annotations (right). **p**, Percentage of each cell type in the high-definition ST assay at \geq 20 μ m and $<$ 20 μ m from A β plaques in nAD and the lecanemab case. **q**, DEGs from myeloid nuclei within $<$ 20 μ m of A β plaques (lecanemab versus nAD). CDR is included as a covariate in the MAST model. **r**, Spatial plots showing *SPP1* expression in binned nuclei around A β plaques in the lecanemab HIPP. **s,t**, Top ten upregulated response DEGs ranked by the average percentile across

microglia and A β differential expression in AN1792 (s) and lecanemab (t). **u**, Top ten combined response genes to AN1792 and lecanemab by summing average percentiles of gene ranks. **v**, Covariate-adjusted Spearman correlation between *TREM2* and *APOE* expression in microglia-enriched gray matter ST spots from AN1792 patients and clinical hallmarks. **b,c,i,k**, Bar plots display means \pm s.e.m. **b,c**, nAD-AN1792 = 3; iAD-lim = 4; iAD-ext = 4; nAD-LCMB = 3; LCMB = 1. **d–f**, nAD-AN1792 = 4; iAD-lim = 6; iAD-ext = 4; nAD-LCMB = 3; LCMB = 1. **g–i**, nAD-AN1792 = 4; iAD = 10; nAD-LCMB = 3; LCMB = 1. **k**, nAD-AN1792 = 4; iAD-lim = 6; iAD-ext = 6; nAD-LCMB = 3; LCMB = 1. **l,m**, nAD-AN1792 = 4; iAD-lim = 6; nAD-LCMB = 3; LCMB = 1. **n,p–q**, nAD = 2; LCMB = 1. **v**, iAD = 13. **g,h,l,m,q**, MAST was used to compare expression levels. Covariates included sex, age, CDR and gDNA percentage with sample ID as a random effect (g and l); brain region, CDR and gDNA percentage with brain region and sample ID as a random effect (h and m); CDR (q). **i**, DESeq2 was used to compare expression levels. Covariates included sex, age, average genes detected, gDNA percentage (AN1792 versus nAD); average genes detected, brain region and gDNA percentage (lecanemab versus nAD). **v**, Covariates included sex, age, average genes detected and gDNA percentage. **g–i,l,m,q,v**, *P* values were FDR adjusted using Benjamini–Hochberg. **b,c,k**, Statistical tests, guided by Shapiro–Wilk and *F* tests, included *t*-tests, Mann–Whitney tests, analysis of variance (ANOVA) with Tukey's test, Welch's ANOVA with Dunnett's T3 test and Kruskal–Wallis with Dunn's test. AN1792-ext, AN1792 immunized with extensive A β clearance; AN1792-lim, AN1792 immunized with limited A β clearance; DE, differential expression; ECs, endothelial cells; Mono, monocytes.

myeloid cells in the lecanemab-treated brain (Extended Data Fig. 4g). Additionally, A β niches in all regions except the FCX shared upregulated genes involved in lysosomal function and protein degradation (*CTSB*),

iron storage (*FTH1*, *FTL*) and extracellular matrix remodeling during inflammation (*CHI3L1*). *A2M* was upregulated in TCX and HIPP A β niches. We also observed *A2M* localized to IBA1 $^{+}$ myeloid cells around



A β deposits (Extended Data Fig. 4h). Notably, we found upregulation of *SPP1* and *FTH1* across A β niches in all brain regions. Pathway analysis of A β -rich ST spots in the TCX revealed upregulation of complement signaling pathways (Fig. 4f). Intriguingly, adipogenesis pathways increased across all regions, suggesting involvement in lipid metabolism processes (Fig. 4f).

We next evaluated immune responses at the protein level within cortical A β niches. We adapted our ST method to include 31 barcoded antibodies targeting immune proteins, which were transferred with RNA probes to generate spatial proteogenomics data. We assessed differentially expressed proteins (DEPs) with or without corresponding DEG transcripts (Fig. 4g). Among DEPs, HLA class II histocompatibility antigen, DR alpha chain (HLA-DRA) was upregulated in A β -rich ST spots across all brain regions (Fig. 4g). Proteins linked to the microglial phagocytic response, such as CD11c and CD68, were upregulated in the TCX and HIPP. IHC revealed numerous CD68 $^{+}$ lysosomal structures within IBA1 $^{+}$ microglia surrounding A β deposits in the HIPP (Fig. 4h and Extended Data Fig. 4i). Interestingly, the immune-inhibitory receptor ligand programmed cell death 1 ligand 1 (PD-L1) was reduced in regions with the highest A β clearance (TCX, PCX).

We used LOESS to assess nonlinear expression changes within A β -rich ST spots in the lecanemab-treated brain (Extended Data Fig. 4j,k). We identified 11 clusters (Extended Data Fig. 4l), with cluster 3 being most associated with immune pathways, including high complement and IL-2–STAT5 signaling (Extended Data Fig. 4m). Cluster 3 was notably upregulated in ST spots with the highest A β content in the lecanemab case, and included previously identified genes such as *A2M*, *APOE*, *APOC1*, *CTSB*, *CD68*, *FCCBP1*, *ITGAX*, *SPP1* and *TREM2* (Fig. 4i,j and Extended Data Fig. 4n). In summary, proteogenomic analysis of the A β niche identified microglial states linked to A β clearance in a patient with AD who was treated with lecanemab.

Shared microglial response drives A β clearance after immunization

To identify common and distinct microglial responses to A β after active and passive immunization, we integrated analyses of all tissues. We quantified A β coverage in the gray matter, confirming a decrease in coverage associated with immunization (Fig. 5a, b). Additionally, we observed increased myeloid recruitment to A β (Fig. 5c). To examine cellular responses to A β , we integrated and clustered cortical gray matter A β -rich ST spots (Fig. 5d and Extended Data Fig. 5a,b). This yielded nine distinct A β niche clusters based on gene expression (Fig. 5e and Extended Data Fig. 5c). We hypothesized that these differences were driven by distinct cellular microenvironments and tested this by using C2L to predict cell-type abundances from our integrated scRNA-seq atlas (Extended Data Fig. 5d). The cortical A β -6 cluster, enriched in microglia, was most prominent in the lecanemab sample, followed by a lesser increase in AN1792 samples (Fig. 5f). This cluster was defined by expression of *A2M*, *APOE*, *C1QC*, *C3*, *SPP1* and others (Extended Data Fig. 5e). Thus, the cortical A β -6 cluster likely represents A β -rich ST spots with recruited myeloid cells. In AN1792 samples with limited A β clearance and in lecanemab-treated brain regions, this cluster showed higher microglia abundance of Mg-2 and Mg-4 compared to nAD controls (Extended Data Fig. 5f).

Differential expression analysis of A β -6 ST spots between AN1792 and nAD samples identified upregulation of *FAM107A*, *RAB13*, *TREM2* and others in AN1792 samples (Fig. 5g and Extended Data Fig. 5g). In lecanemab-treated ST spots, we observed upregulation of *A2M*, *APOE* and others (Fig. 5h and Extended Data Fig. 5g). *SPP1* lacked zero counts, making the MAST hurdle model unsuitable. Using DESeq2, we revealed that *SPP1* was highly upregulated in lecanemab-treated cortical A β -6 ST spots (Fig. 5i). We plotted previously identified microglial subtypes in A β -rich ST spots, finding enrichment of Mg-2 and Mg-4 microglia subtypes in A β niches of lecanemab-treated brain areas (Fig. 5j,k and Extended Data Fig. 5h). Gene expression analysis of A β -associated Mg-2

and Mg-4 ST spots showed increased *APOE* and *FAM107A* in AN1792 samples (Fig. 5l) and upregulated *APOE*, *LIPA*, *SPP1* and *TREM2* among lysosomal function and iron metabolism genes in lecanemab-treated regions (Fig. 5m). Pseudobulked fold changes showed that *FAM107A* is uniquely increased in Mg-2 and Mg-4 A β -associated ST spots in AN1792 samples, while *SPP1* and *LIPA* are associated only with lecanemab treatment (Extended Data Fig. 5i). Notably, *APOE* and *TREM2* increased after both treatments (Extended Data Fig. 5i). Using CellChat⁴⁵, we mapped cell-to-cell signaling related to *APOE*, complement and *SPP1* pathways, identifying increased microglial signaling via complement and *SPP1* pathways in the lecanemab-treated brain, and elevated *APOE* signaling in both lecanemab and AN1792 samples (Extended Data Fig. 5j).

To achieve single-cell resolution, we applied high-definition ST to the HIPP of the lecanemab-treated brain and nAD controls (Extended Data Fig. 5k). Nuclei were segmented⁴⁶, clustered and annotated by top markers (Fig. 5n and Extended Data Fig. 5k,o). We mapped nuclei to A β plaques using immunofluorescence staining (Fig. 5o). Myeloid cells, putative microglia, were overrepresented within 20 μ m of A β plaques in the lecanemab-treated brain but not in nAD controls (Fig. 5o,p). Differential expression analysis confirmed increased expression of *SPP1*, *APOE* and others in microglia near A β plaques after lecanemab treatment (Fig. 5q). *SPP1* expression was localized to nuclei around A β (Fig. 5r). These data validate many of the lower-resolution ST findings throughout the study.

Finally, to identify common and distinct gene expression changes in microglia and at the A β plaque niche from AN1792-treated (Figs. 1m, 2e and 5g,l) and lecanemab-treated (Extended Data Fig. 4f and Figs. 3i and 5h,m) brains, we ranked genes by probabilistic fold change (PFC) and assigned percentile ranks. In AN1792 samples, *FAM107A* was the top response gene, followed by ATP synthase inhibitory factor subunit 1 (*ATPSIF1*), *TREM2* and *APOE* (Fig. 5s and Extended Data Fig. 5p). In lecanemab-treated brain areas, *CHI3L1*, *F3*, *HMOX1* and *SPP1* were the top induced genes (Fig. 5t and Extended Data Fig. 5q). Notably, *TREM2* and *APOE* emerged as common responsive genes in both treatments (Fig. 5u). Our analysis highlights both distinct (*FAM107A*, *SPP1*) and common (*APOE*, *TREM2*) microglial response genes related to active and passive A β immunization.

We correlated *TREM2* and *APOE* expression with clinical data for AN1792 patients, finding a positive correlation between AN1792 antibody titer and *TREM2/APOE* expression in microglia-enriched ST spots (Fig. 5v). There was also a trend toward a negative correlation between *APOE* expression and A β plaque score assessed throughout the neocortex using a standardized method¹⁶. This shows that the expression levels of microglial *APOE* and *TREM2* were directly associated with the immunization response and A β clearance. Altogether, our findings delineate the microglial response mediating A β clearance in AD brains immunized against A β .

Discussion

This study defines the microglial response to A β immunization in patients with AD. We detected upregulation of *APOE* and *TREM2* in microglia of both actively and passively immunized brains. Notably, side effects from passive immunization are more common in *APOE* ε4 carriers^{9,14,47}, and antibodies targeting *TREM2* have been explored as therapeutic strategies for AD^{48,49}. Our findings indicate that *APOE* and *TREM2* play crucial roles in microglial responses to A β immunization, suggesting the microglial response influences both efficacy and risk of adverse effects.

We observed a decrease in the expression of genes related to protein folding and cellular stress in microglia of iAD brains, indicating a more favorable cerebral environment after immunization. Further, we observed elevated expression of neuroprotective genes, including *FGFR3*, in microglia-enriched ST spots of extensively cleared brains. *FGFR3*-*FGF2* signaling may facilitate beneficial neuronal–microglial communication and support neuronal health in cleared A β regions.

Our data also indicate a metabolic shift in microglia during A β immunization. In brains with extensive A β clearance, we found increased oxidative phosphorylation and reduced glycolysis in microglia. This suggests that active immunization can mitigate chronic neuroinflammation in AD and reestablish homeostasis in brains with extensive A β clearance.

To examine passive immunization, we studied a patient with *APOE* ϵ 4 homozygous AD who was treated with lecanemab. Our scRNA-seq analysis revealed increased presence of two microglial subtypes in regions with the highest A β clearance. Both subtypes spatially associated with A β plaques and expressed DAM markers (for example, *APOE* and *TREM2*) and showed elevated complement signaling. Yet, these subtypes differed in their expression of homeostatic markers, as well as their expression of *AXL*, *C3* and *CD74*. Complement signaling, particularly C3, plays a role in A β clearance by aiding A β recognition and phagocytosis by microglia.⁵⁰

Comparative analysis of active and passive immunization revealed that residual A β niches and microglia in the lecanemab brain uniquely upregulated *CHI3L1* and *SPP1* signaling, while AN1792 treatment upregulated *FAM107A* and *ATPSIF1*. Lecanemab-treated brain areas also showed increased expression of lysosomal and protein degradation genes. Both treatments increased *APOE* and *TREM2* expression and reduced HSP-coding genes and stress-responsive microglial states.

Importantly, we found that *APOE* and *TREM2* expression in microglia-enriched ST spots correlated positively with anti-AN1792 antibody titer and trended toward a negative correlation with A β plaque load. This suggests that a more robust and sustained immune response to vaccination is linked to long-term microglial *APOE* and *TREM2* expression and enhanced A β clearance. These findings support the hypothesis that microglial *APOE* and *TREM2* are instrumental in sustained A β clearance following immunization.

Few studies have reported postmortem cases of lecanemab-treated patients.^{18,51} Our study includes one rare case with multifocal intracerebral hemorrhage. Therefore, future studies with larger sample sizes and longitudinal designs are needed to validate and extend our findings related to passive immunization. Animal models can further dissect the mechanistic role of our key microglial markers in A β clearance. Additionally, the effects of *APOE* genotype and sex on immune responses to A β immunization warrant further investigation. Despite the limited sample size, our analysis of rare human samples provides valuable insights into the molecular mechanisms driving A β clearance and suggest potential targets for enhancing immunotherapy efficacy.

In summary, we reveal distinct microglial phenotypes linked to A β immunization in the AD brain. These findings provide new insights into the microglial mechanisms underlying A β clearance and lay the foundation for refining next-generation immunotherapies in AD.

Online content

Any methods, additional references, Nature Portfolio reporting summaries, source data, extended data, supplementary information, acknowledgements, peer review information; details of author contributions and competing interests; and statements of data and code availability are available at <https://doi.org/10.1038/s41591-025-03574-1>.

References

- Karran, E. & Hardy, J. Antiamyloid therapy for Alzheimer's disease—are we on the right road? *N. Engl. J. Med.* **370**, 377–378 (2014).
- Brody, D. L. & Holtzman, D. M. Active and passive immunotherapy for neurodegenerative disorders. *Annu. Rev. Neurosci.* **31**, 175–193 (2008).
- Holmes, C. et al. Long-term effects of A β_{42} immunisation in Alzheimer's disease: follow-up of a randomised, placebo-controlled phase I trial. *Lancet* **372**, 216–223 (2008).
- Nicoll, J. A. et al. Neuropathology of human Alzheimer disease after immunization with amyloid-beta peptide: a case report. *Nat. Med.* **9**, 448–452 (2003).
- Nicoll, J. A. et al. A β species removal after A β_{42} immunization. *J. Neuropathol. Exp. Neurol.* **65**, 1040–1048 (2006).
- Salloway, S. et al. Two phase 3 trials of bapineuzumab in mild-to-moderate Alzheimer's disease. *N. Engl. J. Med.* **370**, 322–333 (2014).
- Liu, E. et al. Amyloid-beta 11C-PiB-PET imaging results from 2 randomized bapineuzumab phase 3 AD trials. *Neurology* **85**, 692–700 (2015).
- Chen, T. et al. Results from the long-term extension of PRIME: a randomized phase 1b trial of aducanumab. *Alzheimers Dement.* **20**, 3406–3415 (2024).
- van Dyck, C. H. et al. Lecanemab in early Alzheimer's disease. *N. Engl. J. Med.* **388**, 9–21 (2023).
- Orgogozo, J. M. et al. Subacute meningoencephalitis in a subset of patients with AD after Abeta42 immunization. *Neurology* **61**, 46–54 (2003).
- Gilman, S. et al. Clinical effects of A β immunization (AN1792) in patients with AD in an interrupted trial. *Neurology* **64**, 1553–1562 (2005).
- Bayer, A. J. et al. Evaluation of the safety and immunogenicity of synthetic A β_{42} (AN1792) in patients with AD. *Neurology* **64**, 94–101 (2005).
- Ferrer, I., Boada Rovira, M., Sanchez Guerra, M. L., Rey, M. J. & Costa-Jussa, F. Neuropathology and pathogenesis of encephalitis following amyloid-beta immunization in Alzheimer's disease. *Brain Pathol.* **14**, 11–20 (2004).
- Salloway, S. et al. Amyloid-related imaging abnormalities in 2 phase 3 studies evaluating aducanumab in patients with early Alzheimer disease. *JAMA Neurol.* **79**, 13–21 (2022).
- Salloway, S. et al. A phase 2 multiple ascending dose trial of bapineuzumab in mild to moderate Alzheimer disease. *Neurology* **73**, 2061–2070 (2009).
- Nicoll, J. A. R. et al. Persistent neuropathological effects 14 years following amyloid-beta immunization in Alzheimer's disease. *Brain* **142**, 2113–2126 (2019).
- Reish, N. J. et al. Multiple cerebral hemorrhages in a patient receiving Lecanemab and treated with t-PA for stroke. *N. Engl. J. Med.* **388**, 478–479 (2023).
- Castellani, R. J. et al. Neuropathology of anti-amyloid-beta Immunotherapy: a case report. *J. Alzheimers Dis.* **93**, 803–813 (2023).
- Corder, E. H. et al. Gene dose of apolipoprotein E type 4 allele and the risk of Alzheimer's disease in late onset families. *Science* **261**, 921–923 (1993).
- Strittmatter, W. J. et al. Apolipoprotein E: high-avidity binding to beta-amyloid and increased frequency of type 4 allele in late-onset familial Alzheimer disease. *Proc. Natl Acad. Sci. USA* **90**, 1977–1981 (1993).
- Butler, A. W. et al. Meta-analysis of linkage studies for Alzheimer's disease—a web resource. *Neurobiol. Aging* **30**, 1037–1047 (2009).
- Guerreiro, R. et al. *TREM2* variants in Alzheimer's disease. *N. Engl. J. Med.* **368**, 117–127 (2013).
- Krasemann, S. et al. The *TREM2-APOE* pathway drives the transcriptional phenotype of dysfunctional microglia in neurodegenerative diseases. *Immunity* **47**, 566–581 (2017).
- Keren-Shaul, H. et al. A unique microglia type associated with restricting development of Alzheimer's disease. *Cell* **169**, 1276–1290 (2017).
- Gerrits, E. et al. Distinct amyloid-beta and tau-associated microglia profiles in Alzheimer's disease. *Acta Neuropathol.* **141**, 681–696 (2021).
- Nguyen, A. T. et al. APOE and *TREM2* regulate amyloid-responsive microglia in Alzheimer's disease. *Acta Neuropathol.* **140**, 477–493 (2020).

27. Hartl, F. U., Bracher, A. & Hayer-Hartl, M. Molecular chaperones in protein folding and proteostasis. *Nature* **475**, 324–332 (2011).
28. Murshid, A., Prince, T. L., Lang, B. & Calderwood, S. K. Role of heat shock factors in stress-induced transcription. *Methods Mol. Biol.* **1709**, 23–34 (2018).
29. Finak, G. et al. MAST: a flexible statistical framework for assessing transcriptional changes and characterizing heterogeneity in single-cell RNA sequencing data. *Genome Biol.* **16**, 278 (2015).
30. Hasegawa, H. et al. Microglial signaling by amyloid beta protein through mitogen-activated protein kinase mediating phosphorylation of MARCKS. *Neuroreport* **12**, 2567–2571 (2001).
31. Schmidt, M. V. et al. Tumor suppressor down-regulated in renal cell carcinoma 1 (DRR1) is a stress-induced actin bundling factor that modulates synaptic efficacy and cognition. *Proc. Natl Acad. Sci. USA* **108**, 17213–17218 (2011).
32. Kleshchevnikov, V. et al. Cell2Location maps fine-grained cell types in spatial transcriptomics. *Nat. Biotechnol.* **40**, 661–671 (2022).
33. Fujita, M. et al. Cell subtype-specific effects of genetic variation in the Alzheimer's disease brain. *Nat. Genet.* **56**, 605–614 (2024).
34. Green, G. S. et al. Cellular communities reveal trajectories of brain ageing and Alzheimer's disease. *Nature* **633**, 634–645 (2024).
35. Noda, M. et al. FGF-2 released from degenerating neurons exerts microglial-induced neuroprotection via FGFR3-ERK signaling pathway. *J. Neuroinflammation* **11**, 76 (2014).
36. Haure-Mirande, J. V., Audrain, M., Ehrlich, M. E. & Gandy, S. Microglial TYROBP/DAP12 in Alzheimer's disease: transduction of physiological and pathological signals across TREM2. *Mol. Neurodegener.* **17**, 55 (2022).
37. Venegas, C. et al. Microglia-derived ASC specks cross-seed amyloid-beta in Alzheimer's disease. *Nature* **552**, 355–361 (2017).
38. Maxeiner, S. et al. Crucial role for the LSP1-myosin1e bimolecular complex in the regulation of Fcγ receptor-driven phagocytosis. *Mol. Biol. Cell* **26**, 1652–1664 (2015).
39. Lujan, D. A., Ochoa, J. L. & Hartley, R. S. Cold-inducible RNA binding protein in cancer and inflammation. *Wiley Interdiscip. Rev. RNA* <https://doi.org/10.1002/wrna.1462> (2018).
40. Su, F. et al. CIRBP ameliorates neuronal amyloid toxicity via antioxidative and antiapoptotic pathways in primary cortical neurons. *Oxid. Med. Cell Longev.* **2020**, 2786139 (2020).
41. Sun, N. et al. Human microglial state dynamics in Alzheimer's disease progression. *Cell* **186**, 4386–4403 (2023).
42. Young, M. D. & Behjati, S. SoupX removes ambient RNA contamination from droplet-based single-cell RNA sequencing data. *Gigascience* **9**, giaa151 (2020).
43. McQuade, A. et al. Gene expression and functional deficits underlie TREM2-knockout microglia responses in human models of Alzheimer's disease. *Nat. Commun.* **11**, 5370 (2020).
44. Lawrence, A. R. et al. Microglia maintain structural integrity during fetal brain morphogenesis. *Cell* **187**, 962–980 (2024).
45. Jin, S. et al. Inference and analysis of cell-cell communication using CellChat. *Nat. Commun.* **12**, 1088 (2021).
46. Schmidt, U., Weigert, M., Broaddus, C. & Myers, G. Cell detection with star-convex polygons. *Lect. Notes Comput. Sci.* **11071**, 265–273 (2018).
47. Sims, J. R. et al. Donanemab in early symptomatic Alzheimer disease: the TRAILBLAZER-ALZ 2 randomized clinical trial. *JAMA* **330**, 512–527 (2023).
48. Wang, S. et al. Anti-human TREM2 induces microglia proliferation and reduces pathology in an Alzheimer's disease model. *J. Exp. Med.* **217**, e20200785 (2020).
49. van Lengerich, B. et al. A TREM2-activating antibody with a blood-brain barrier transport vehicle enhances microglial metabolism in Alzheimer's disease models. *Nat. Neurosci.* **26**, 416–429 (2023).
50. Gedam, M. et al. Complement C3aR depletion reverses HIF-1alpha-induced metabolic impairment and enhances microglial response to Abeta pathology. *J. Clin. Invest.* **133**, e167501 (2023).
51. Solopova, E. et al. Fatal iatrogenic cerebral beta-amyloid-related arteritis in a woman treated with lecanemab for Alzheimer's disease. *Nat. Commun.* **14**, 8220 (2023).

Publisher's note Springer Nature remains neutral with regard to jurisdictional claims in published maps and institutional affiliations.

Open Access This article is licensed under a Creative Commons Attribution 4.0 International License, which permits use, sharing, adaptation, distribution and reproduction in any medium or format, as long as you give appropriate credit to the original author(s) and the source, provide a link to the Creative Commons licence, and indicate if changes were made. The images or other third party material in this article are included in the article's Creative Commons licence, unless indicated otherwise in a credit line to the material. If material is not included in the article's Creative Commons licence and your intended use is not permitted by statutory regulation or exceeds the permitted use, you will need to obtain permission directly from the copyright holder. To view a copy of this licence, visit <http://creativecommons.org/licenses/by/4.0/>.

© The Author(s) 2025, corrected publication 2025

Lynn van Olst  ^{1,2}, Brooke Simonton ^{1,2}, Alex J. Edwards ^{1,2}, Anne V. Forsyth ^{1,2}, Jake Boles ^{1,2}, Pouya Jamshidi ³, Thomas Watson ^{1,2}, Nate Shepard ², Talia Krainc ², Benney MR Argue  ^{1,2}, Ziyang Zhang ^{1,2}, Joshua Kuruvilla ^{1,2}, Lily Camp  ^{1,2}, Mengwei Li ⁴, Hang Xu ⁴, Jeanette L. Norman ⁵, Joshua Cahan  ^{1,2}, Robert Vassar ^{2,6}, Jinmiao Chen ^{4,7,8}, Rudolph J. Castellani ³, James AR Nicoll  ^{5,9}, Delphine Boche  ⁵ & David Gate  ^{1,2} 

¹Abrams Research Center on Neurogenomics, Northwestern University Feinberg School of Medicine, Chicago, IL, USA. ²The Ken & Ruth Davee Department of Neurology, Northwestern University Feinberg School of Medicine, Chicago, IL, USA. ³Department of Pathology, Northwestern University Feinberg School of Medicine, Chicago, IL, USA. ⁴Bioinformatics Institute, Agency for Science, Technology and Research, Singapore, Singapore. ⁵Clinical Neurosciences, School of Clinical and Experimental Sciences, Faculty of Medicine, University of Southampton, Southampton, UK. ⁶Mesulam Center for Cognitive Neurology and Alzheimer's Disease, Northwestern University Feinberg School of Medicine, Chicago, IL, USA. ⁷Centre for Computational Biology and Program in Cancer and Stem Cell Biology, Duke-NUS Medical School, Singapore, Singapore. ⁸Immunology Translational Research Program, Department of Microbiology and Immunology, Yong Loo Lin School of Medicine, National University of Singapore, Singapore, Singapore. ⁹Department of Cellular Pathology, University Hospital Southampton National Health Service Trust, Southampton, UK.  e-mail: dgate@northwestern.edu

Methods

Human tissue samples

AN1792 study cohort. Clinical and neuropathologic follow-up of patients with AD enrolled in the Elan Pharmaceuticals phase I trial of AN1792 was previously reported^{3,10–12}. FCX tissue was available from 22 patients with iAD, of whom 16 had a neuropathologic diagnosis of AD. The remaining 6 patients had a different cause of dementia and were excluded from further analysis. Notably, 3 of the 16 AD brains (cases 2, 3 and 9) were omitted due to low RNA quality scores, leaving a final cohort of 13 iAD samples. One patient (case 1) required imaging in life, which demonstrated features of meningoencephalitis¹⁰ and neuroradiological features consistent with the later-defined amyloid related imaging abnormalities (ARIA) edema¹⁶. Within adequate numbers of postmortem placebo-treated samples from the original AN1792 trial, frontal cortices of 6 nAD cases and 6 NND cases were used as controls. Cases were matched as closely as possible for age at death. In total, postmortem FFPE frontal cortical samples of 13 iAD (mean age of death, 79.97 years; range, 63–89 years), 6 nAD controls (mean age of death, 79.60 years; range, 65–89 years) and 6 NND controls (mean age of death, 74.93 years; range, 63–82) were included in the active immunization analysis. All nAD cases and 4 NND FCX samples were sourced from Stanford Alzheimer's Disease Research Center. Two additional NND samples were sourced from Northwestern Pathology. Relevant clinical and demographic information of iAD, nAD and NND cases are listed in Extended Data Table 1. Tissue blocks were cut into 5-μm sections and stored at 4 °C until further use.

Lecanemab and nAD controls. Clinical and neuropathologic findings of a 65-year-old *APOE* ε4/ε4 female patient with early cognitive decline treated with lecanemab were previously reported^{17,18}. In the open-label phase, the patient received three intravenous lecanemab infusions—each 2 weeks apart. Four days after the final dose, the patient developed stroke-like symptoms, received tissue plasminogen activator and suffered fatal intracerebral hemorrhages. Consent was obtained to perform full-body postmortem examination and subsequent reporting of the neuropathologic findings related to her receiving anti-Aβ. Multiple foci of histiocytic/microglial reaction to parenchymal amyloid plaques were noted. According to NIA-AA 2012 consensus guidelines⁵², the AD neuropathologic changes would be categorized as 'high'. FFPE tissue blocks from the FCX, TCX, PCX and HIPP of both donors were sectioned into 5-μm slices and stored at 4 °C. The nAD control samples (mean age at death, 69.3 years; range, 62–82 years) were matched for parenchymal AD pathology (high), vascular AD pathology and *APOE* ε4/ε4 genotype. Notably, one nAD donor also had magnetic resonance imaging-positive microbleeds on gradient echo sequences. Relevant clinical and demographic information of lecanemab and nAD cases are listed in Extended Data Table 2.

Ethics declarations for human tissues

AN1792 tissue. This study was conducted in compliance with all relevant ethical guidelines and was approved by BRAIN UK (UK Brain Archive Information Network) under REC reference 19/SC/0217.

ROSMAP data. All participants in the Religious Orders Study and Rush Memory and Aging Project (ROSMAP) enrolled without known dementia and agreed to detailed clinical evaluation and brain donation at death⁵³. Both studies were approved by an Institutional Review Board (IRB) of Rush University Medical Center (ROS IRB no. L91020181, MAP IRB no. L86121802). Both studies were conducted according to the principles expressed in the Declaration of Helsinki. Each participant signed an informed consent, an Anatomic Gift Act and an RADC Repository consent (IRB no. L99032481) allowing their data and biospecimens to be repurposed.

Lecanemab tissue and nAD controls. Consent was obtained to perform postmortem examination and subsequent reporting of the

neuropathologic findings related to the patient receiving lecanemab. The study of de-identified nAD tissue was approved by the IRB of Northwestern University (exempt IRB no. 00219860).

DNA collection and genotyping

gDNA was extracted from residual brain material on glass slides following ST workflow, using the QIAamp DNA FFPE Tissue Kit (catalog no. 56404, Qiagen), with deparaffinization steps omitted as they were completed during the ST protocol. DNA was isolated from all nAD and NND samples, as well as AN1792 samples 102-19 and 102-20, which lacked *APOE* genotype information. Positive controls were included to validate genotyping. Quality and concentration of extracted DNA were assessed to ensure suitability for genotyping. *APOE* genotyping for the single-nucleotide polymorphisms (SNPs) rs429358 and rs7412 was conducted at the University of Illinois at Chicago Genomics Research Core using the BioMark HD Real-Time PCR system (Fluidigm) and SNP Type assays (rs429358: C_3084793_20; rs7412: C_904973_10; Thermo Fisher). Genotyping was performed according to the manufacturer's protocol, with each SNP assayed using TaqMan SNP Genotyping Assays (Applied Biosystems). Genotype calling was conducted with the SNP Genotyping Analysis software (Fluidigm) using default analysis parameters: a confidence threshold of 65, global normalization and k-means clustering. PCR cycle 35 was used for SNP calling, and each sample was analyzed in three technical replicates. No template controls were incorporated into vacant inlets as negative controls. Allele calls were determined based on fluorescence signals from FAM and VIC probes, and each *APOE* haplotype was assigned by combining the alleles of rs429358 and rs7412, resulting in the following classifications: ε2 (T/T), ε3 (T/C) and ε4 (C/C).

ST

FFPE samples were deparaffinized, stained with H&E and decrosslinked according to the Visium CytAssist Spatial Gene Expression for FFPE protocol (CG000520 rev. B, 10x Genomics). H&E-stained tissues were imaged on an EVOS M7000 Imaging System (AMF7000, Thermo Fisher Scientific) using a ×20 objective (0.45 NA, AMEP4982, Thermo Fisher Scientific). Immediately after decrosslinking, libraries were prepared according to the user guide for Visium CytAssist Spatial Gene Expression Reagent Kits (CG000495, rev. E, 10x Genomics). Final libraries were sequenced by the NUSeq Core at Northwestern University Feinberg School of Medicine using the Illumina NovaSeq 6000 or Illumina NovaSeq X Plus platforms to the recommended depth of 25,000 reads per tissue-covered ST spot. The Space Ranger pipeline version 2.0.0., referencing the GRCh38 human genome (GENCODE v32/Ensembl 98), and Visium Transcriptome Probe Set v2.0 (10x Genomics) were used to process FASTQ files. ST spots were annotated in the Loupe Browser (10x Genomics) using the high-resolution images to delineate meninges, cortical layers and white matter.

Spatial proteogenomics

FFPE samples were deparaffinized, decrosslinked and stained with a combination of DAPI (1:100 dilution; 62248; Thermo Fisher), rabbit anti-IBA1 (1:250 dilution; 019-19741; WAKO) and mouse anti-pan-Aβ (1:250 dilution; clone 4G8; 800708; BioLegend). Notably, we used TrueBlack Plus Lipofuscin Autofluorescence Quencher (23014; Biotium) according to the manufacturer's instructions. Tissues were imaged on an EVOS M7000 Imaging System (AMF7000, Thermo Fisher Scientific) using a ×20 objective (0.45 NA, AMEP4982, Thermo Fisher Scientific, or an Olympus Lucplanfl N ×20/0.45 Ph1UIS2 Collar Fn22). After imaging, spatial gene and protein expression libraries were immediately prepared according to the user guide for Visium CytAssist Spatial Gene and Protein Expression Reagent Kits (CG000494; rev. B; 10x Genomics). We used the Visium Human Transcriptome Probe Set version 2.0 for RNA transcript detection, along with the Human FFPE Immune Profiling Panel, which includes a 35-plex CytAssist Panel of antibodies, both

intracellular and extracellular, sourced from BioLegend and Abcam for protein detection. This panel also comprises four isotype controls. Final libraries were sequenced as detailed above for ST. The targeted sequencing depth was 25,000 reads per tissue-covered ST spot for gene expression libraries, and 5,000 reads per tissue-covered ST spot for protein expression libraries, as recommended. The Space Ranger pipeline version 2.1.1., referencing the GRCh38 human genome (GENCODE v32/Ensembl 98), and Visium Transcriptome Probe Set v2.0 (10x Genomics) were used to process FASTQ files. ST spots were annotated in the Loupe Browser (10x Genomics) using the high-resolution images to delineate meninges, cortical layers and white matter, and to exclude hemorrhagic regions.

High-definition ST

FFPE samples were deparaffinized, decrosslinked and stained with DAPI, rabbit anti-pan-A β (1:500 dilution; clone D54D2, 8243, Cell Signaling Technology), goat anti-IBA1 (1:100 dilution; ab5076, Abcam) and mouse anti-phospho-Tau (1:250 dilution; MN1020, Thermo Fisher) according to the Visium HD FFPE Tissue Preparation Handbook (CG000684 rev. A, 10x Genomics). Lipofuscin autofluorescence was quenched with TrueBlack Lipofuscin Quencher. Stained tissues were imaged on an EVOS M7000 Imaging System (AMF7000, Thermo Fisher Scientific) using a $\times 20$ objective (Olympus Lucplanfl N $\times 20/0.45$ Ph1 UIS2 Collar Fn22). Immediately following decrosslinking, libraries were prepared per the Visium HD Spatial Gene Expression Reagent Kits user guide (CG000685 rev. B, 10x Genomics). Final libraries were sequenced by the NUSeq Core at Northwestern University Feinberg School of Medicine on an Illumina NovaSeq X Plus platform to a target depth of 275 million reads per fully covered capture area. FASTQ files were processed using the Space Ranger pipeline version 3.0.0, referencing the GRCh38 human genome (GENCODE v32/Ensembl 98) and Visium Transcriptome Probe Set v2.0 (10x Genomics).

scRNA-seq

For each sample, 1–2 consecutive FFPE scrolls of 25 μ m were prepared and processed according to the Isolation of Cells from FFPE Tissue Sections for Chromium Fixed RNA Profiling protocol (CG000632, 10x Genomics). After deparaffinization and dissociation by pestle, single cells were hybridized with barcoded probes overnight. GEM generation and library construction were performed as outlined in the Chromium Fixed RNA Profiling Reagent Kits for Multiplexed Samples manual (CG000527; rev. E; 10x Genomics). The first batch included four brain regions—FCX, TCX, PCX and HIPP—from one nAD control (NMA22-300) and one lecanemab-treated sample (NMA22-205). The second batch contained the same regions from two additional nAD controls (A14-193 and A11-170). The third batch contained FCX samples from ten ANI792 samples (102-1, 102-7, 102-8, 102-11, 102-15, 102-16, 102-17, 102-19, 102-21 and 102-22). To enhance cell yield per tissue, samples were split across 2 barcodes per pool, totaling 16 barcodes. Limited cell numbers in samples 102-7, 102-8, 102-11 and 102-21 restricted them to a single barcode each. We targeted approximately 8,000 cells per barcode, aiming for a total of 16,000 cells per tissue per pool. For batches one and three, two pools were generated, targeting 32,000 cells across both pools for samples with dual barcodes. Cell counts were taken at several stages to ensure consistent pooling, using a DAPI stain (1:2,000 dilution; 62248; Thermo Fisher) and imaged with an EVOS M7000 Imaging System (AMF7000, Thermo Fisher Scientific) using a $\times 4$ objective lens (0.13 NA, AMEP4980, Thermo Fisher Scientific). The final libraries were indexed and pooled, and then sequenced together by the NUSeq Core at Northwestern University Feinberg School of Medicine on an Illumina NovaSeq X Plus sequencer, aiming for approximately 25,000 reads per cell. Demultiplexed FASTQ files were processed using the Cell Ranger pipeline version 7.2.0, referencing the GRCh38 human genome (GENCODE v32/Ensembl 98) and the Visium Transcriptome Probe Set v2.0 (10x Genomics).

IHC

DAB hematoxylin staining. Consecutive sections from the ST data, spaced 5–10 μ m apart, were used to stain for pan-A β . FFPE sections were heated at 60 °C for 1 h, followed by incubation in xylenes and a graded ethanol series. Antigen retrieval was performed at 95 °C for 30 min in either citrate buffer pH 6.0 (64142-08, Electron Microscopy Sciences) or Tris-EDTA pH 9.0 (AB93684, Abcam). Slides were blocked using 10% normal goat serum (ab7481, Abcam) in PBS with 0.03% Triton-X (21568-2500, Acros Organics) for up to 4 h. The sections were then incubated overnight at 4 °C with the primary antibody for pan-A β (1:100 dilution; clone D54D2, 8243, Cell Signaling) and subsequently with goat anti-rabbit horseradish peroxidase (1:200 dilution; P0448, Agilent Technologies) for 1 h at room temperature. Sections were then treated with diluted DAB chromogen (K3468, Dako) for 20 min at room temperature. Hematoxylin (51275, Sigma-Aldrich) was used for counterstaining before the sections were dehydrated and mounted with Cytoseal (8312-4, Epredia). Nonadjacent serial sections were also stained for phosphorylated tau using the AT8 antibody (1:500 dilution; Thermo Fisher Scientific, MN1020) using this protocol.

Immunofluorescence

FFPE sections were placed in an oven for 1 h at 60 °C before deparaffinization in xylenes and rehydration with a series of graded ethanol. Antigen retrieval was performed at 95 °C for 30 min in citrate buffer (pH 6.0; 64142-08, Electron Microscopy Sciences) or Tris-EDTA buffer (pH 9.0; Ab93684, Abcam). Slides were blocked using 10% of normal donkey serum (017-000-121, Jackson ImmunoResearch; Ab7475, Abcam) in PBS with 0.03% Triton-X (21568-2500, Acros Organics) for up to 4 h. Sections were then incubated with primary antibodies (Extended Data Table 3) overnight at 4 °C, followed by a 1-h incubation in Alexa Fluor-labeled secondary antibodies (1:400 dilution) at room temperature. Primary antibodies used included goat anti-IBA1 (1:150 dilution; ab5076, Abcam), rabbit anti-A β (1:1,000 dilution; clone D54D2, 8243, Cell Signaling), mouse anti-CD68 (1:400 dilution; clone KP1, ab955, Abcam), rabbit anti-IBA1 (1:400 dilution; 019-19741, WAKO), goat anti-APOE (1:500 dilution; ab947, Sigma-Aldrich), mouse anti-A β (1:1,000 dilution; clone D3D2N, 15126, Cell Signaling), rabbit anti-TMS1/ASC (1:400 dilution; clone RM1049, ab309497, Abcam), mouse anti-A β (1:250 dilution; clone 4G8, 800708, BioLegend), rabbit anti-A2M (1:500 dilution; clone EPR4432, ab109422, Abcam), rabbit anti-APOC1 (1:300 dilution; clone EPRI6813, ab198288, Abcam) and rabbit anti-SPP1 (1:300 dilution; ab8448, Abcam). Immunofluorescence-stained slides were counterstained for DNA using DAPI (1:5,000 dilution; 62248, Thermo Fisher), followed by quenching of autofluorescence with TruBlack Plus (1:40 dilution; 23014, Biotium) in PBS. Slides were mounted using ProLong Gold Antifade Mountant (P36934; Fisher Scientific).

Imaging analysis

Imaging and processing of pan-A β DAB stains in consecutive ST images. Tissue imaging was performed with a TissueGnostics slide scanner. The acquired images were processed using Fiji software (National Institutes of Health (NIH)). Briefly, deconvolution was applied to the images for the hematoxylin and DAB staining. Manual thresholds were set for A β reactivity using the DAB stain by a researcher blinded to sample identification. The derived binary signal was further cleaned by removing small particles. A β coverage in the gray matter was determined by calculating the ratio of A β deposits in the gray matter to the total area of the gray matter per sample. To construct the expanded A β niches, the binary A β signal was artificially extended by 100 μ m from its original boundary, with a gradual decrease in signal intensity noted every 20 μ m. Subsequently, the images were aligned to the CytAssist image using the Loupe browser (version 7.0.1, 10x Genomics) and further integrated with the spatial RNA data using Space Ranger version 2.1.1. Importantly, ST spots with unreliable A β staining, arising from technical issues or tissue anomalies such as folds or holes, were

omitted from subsequent A β niche analyses. Additionally, vascular A β ST spots were excluded from any further analyses.

Imaging and processing of phosphorylated Tau (AT8) DAB stains. Tissue imaging for AT8-stained slides was performed at $\times 20$ magnification using an automated slide scanner microscope (Olympus VS110, Olympus America) at the Biomedical Imaging Unit, Faculty of Medicine, University of Southampton. The acquired images were processed using Fiji software (NIH). Briefly, deconvolution was applied to separate the hematoxylin and DAB signals. Manual thresholds were set for AT8 reactivity in the DAB channel by a researcher blinded to sample identification. The resulting binary signal was refined by removing small particles. AT8 coverage in the gray matter was quantified as the ratio of AT8-positive area to the total gray matter area per sample.

Processing of immunofluorescence images for spatial proteogenomics. High-resolution imaging in the spatial proteogenomic workflow was conducted using Fiji. The DAPI channel was auto-thresholded using the Li vector, with subsequent removal of entities larger than >1 cm and application of the watershed function to separate binary nuclear masks. The IBA1 channel processing involved dividing the image into a 25×25 grid, applying Bleach Correction via Histogram Matching to each segment, reassembling the image and using the RollingBall algorithm (radius, $2.8 \mu\text{m}$) to reduce background noise. Both IBA1 and A β channels underwent manual thresholding, conducted by a researcher blinded to sample identification. After binarization, channels were subjected to two rounds of dilation and erosion, followed by a filtering step to remove oversized objects in A β and IBA1, targeting noise reduction. The binarized IBA1 masks were then utilized to refine the bleach-corrected IBA1 channel. This refinement was achieved by overlaying the binarized IBA1 mask onto the bleach-corrected IBA1 channel. In this process, only the regions within the confines of the binarized mask were retained, while areas outside the mask were cleared.

Vascular and cortical A β were identified in the high-resolution images from the spatial proteogenomic workflow using the LabKit machine learning tool³⁴ within Fiji. Each sample was analyzed with a unique classifier to generate a vascular A β probability map. This map was initially enhanced with despeckling and Gaussian blur ($\sigma = 4$) to improve smoothness, followed by triple dilation and erosion and filtering to exclude small particles. The probability maps were then manually thresholded by a researcher blinded to sample identification. Observations of vascular A β missed by the automated process but detected upon visual inspection were carefully annotated and included. The vascular A β binary signal was dilated twice before being extracted from the processed A β channel, leaving the residual signal to be identified as cortical A β . Expanded A β niches were subsequently delineated as described above. For nAD controls A14-193 and A11-170, vascular A β was manually annotated instead of using LabKit. Importantly, ST spots exhibiting unreliable A β staining, whether due to technical complications or the presence of tissue folds or holes, were excluded from further analyses related to the A β niche.

A β coverage and IBA1 colocalization. The coverage of cortical or total A β within the gray matter was determined by calculating the percentage of the area covered by the binarized cortical or total A β mask in the gray matter to the total area of the gray matter for each brain region per donor. To evaluate the association between IBA1 $^+$ cells and cortical or total A β , the area where cortical A β and IBA1 colocalized was divided by the total area of cortical or total A β present in the gray matter.

Data preprocessing, quality control and integration

AN1792 RNA for ST. Seurat objects were initialized for each sample with Space Ranger's filtered feature barcode matrices using Load10X_Spatial. ST spots with extremely high or low unique molecular identifier (UMI) counts or extremely low feature counts were removed on a

per-sample basis. Outermost ST slide spots, ST spots with at least 20% mitochondrial expression and ST spots that were not covering tissue were removed. Raw counts were independently normalized using log-normalization and SCTransform normalization, with SCTransform models fit per sample. Depending on the assay, raw counts, log-normalized data or SCTransformed data were utilized.

scRNA-seq. Cell Ranger's filtered feature barcode matrices for each sample in each pool were corrected for background contamination using SoupX⁴². Low-quality cells were removed before doublet identification, using a sample-specific and pool-specific minimum UMI threshold of three median absolute deviations below the median and a minimum feature threshold of two median absolute deviations below the median. Additionally, cells exhibiting mitochondrial gene expression above 20% were removed. Doublet identification was performed with DoubletFinder utilizing ten principal components, a pN setting of 0.25 and a pool-specific predicted doublet rate determined based on the average number of cells loaded per probe barcode, with a 0.4% undetectable multiplet rate for 825 cells loaded per barcode as per the Chromium Fixed RNA Profiling Reagent Kits for Multiplexed Samples manual (CG000527; rev. E; 10x Genomics). Doublets were removed, and samples from AN1792 donors 102-1, 102-16, 102-17, 102-19 and 102-22 were retained, while donors 102-7, 102-8, 102-11 and 102-21 were excluded due to high contamination fractions, low UMI counts or high mitochondrial expression. The remaining raw counts were further processed with SCTransform while adjusting for mitochondrial gene expression, with SCTransform models fit for each sample in each pool. Fifty principal components were derived from the SCTransform-processed data, which was then harmonized across both pools and samples using the IntegrateLayers function with the HarmonyIntegration approach. Lastly, UMAP visualization was constructed from 30 integrated features.

Lecanemab RNA for ST. Seurat objects were initialized for each sample with Space Ranger's filtered feature barcode matrices using Load10X_Spatial. ST spots with extremely high or low UMI counts or extremely low feature counts were removed on a per-sample basis. ST spots with at least 20% mitochondrial expression were removed for FCX, TCX and PCX and ST spots with at least 30% mitochondrial expression were removed for HIPP. ST spots not located on cortical or hippocampal tissue were excluded. Outermost ST slide spots, and ST spots with zero protein expression were removed. Raw counts were independently normalized using log-normalization and SCTransform normalization, with SCTransform models fit per sample. Depending on the assay, raw counts, log-normalized data or SCTransformed data were utilized.

Lecanemab spatial protein analysis. For each sample, Seurat objects were created from Space Ranger's filtered feature barcode matrices, which included isotype-normalized counts, via the Load10X_Spatial function. Isotype control antibodies were excluded from further analysis.

High-definition ST analysis. Nuclei segmentation was performed using StarDist⁴⁶, with expression data from Space Ranger's $2 \times 2\text{-}\mu\text{m}$ filtered feature barcode matrices assigned to segmented nuclei. Nuclei with fewer than ten UMI counts or over 20% mitochondrial expression were excluded. Raw counts were transformed with SCTransform, with SCTransform models fit per sample. Fifty principal components were derived from the SCTransform-processed data. Integration across samples was achieved with IntegrateLayers using the HarmonyIntegration method, and a UMAP was generated using 30 integrated features.

snRNA-seq integration and reference generation

A snRNA-seq dataset^{33,34} from ROSMAP⁵³ was used to generate a reference atlas for ST data. We initially identified 5,000 feature genes

per batch in Seurat using `FindVariableFeatures`. From this pool of genes, we selected 5,000 common feature genes across all datasets for anchor identification using the `FastFindAnchors` function from the `FastIntegration` package⁵⁵. The resulting batch-corrected values were subsequently used for downstream analyses, including principal component analysis, UMAP and clustering. For annotation of broad cell types, we utilized the feature genes identified during the integration stage. Subsequently, within each broad cell type, we reselected feature genes and conducted similar analyses to delineate detailed subtypes. Major cell types used were astrocytes, endothelial cells, stromal cells, immune cells, oligodendrocytes, oligodendrocyte precursor cells, interneurons, ENs, fibroblasts, pericytes and smooth muscle cells. We then randomly downsampled 2,000 cells per cell type, or included all cells for categories with fewer than 2,000 cells, resulting in a reference dataset of 34,695 cells.

Cell-type annotation

scRNA-seq. Clustering was conducted in Seurat by first applying the `FindNeighbors` function with 30 integrated features, followed by `FindClusters` at multiple resolutions, with a final resolution of 1 used to define initial clusters. To identify immune subtypes, the data were subsetted to clusters expressing immune markers. Data from different cohorts was merged, and raw counts were transformed using `SCTransform`, while adjusting for mitochondrial gene expression, with `SCTransform` models fit per cohort. Fifty principal components were generated from the `SCTransform` data, and integration across cohorts was performed using `IntegrateLayers` with the CCA integration method. Clustering was refined by reapplying `FindNeighbors` and `FindClusters` with 30 integrated features, defining immune clusters at a resolution of 0.35. A UMAP was generated using the 30 integrated features.

A β niches. Data from all cohorts were subsetted to include cortical A β -rich ST spots in gray matter. Raw counts were transformed using `SCTransform`, with `SCTransform` models fit per sample and 50 principal components were generated from `SCTransform` data. Integration across samples was conducted using `IntegrateLayers` with the `HarmonyIntegration` method. A UMAP was generated with 30 integrated features, followed by clustering with Seurat's `FindNeighbors` and `FindClusters` functions across various resolutions. Final clusters were defined at a resolution of 0.4.

High-definition ST. Clustering of Visium HD data was conducted in Seurat using `FindNeighbors` with 30 integrated features, followed by `FindClusters` across multiple resolutions, with final clusters defined at a resolution of 0.2.

ST deconvolution

For spatial deconvolution, we utilized the `C2L` (v0.1.3) package³². Gene filtering on the reference data was conducted using the `filter_genes` function, with parameters set to `cell_count_cutoff = 5`, `cell_percentage_cutoff2 = 0.03` and `nonz_mean_cutoff = 1.12`. The `batch_key` parameter was configured as sequencing batch for the scRNA-seq atlas and sample ID for the scRNA-seq atlas, with each sample ID corresponding to a specific brain region (for example, the same donor had a distinct sample ID for each brain region). The reference regression model was trained for 500 epochs for the reference atlas and 750 epochs for our in-house-created scRNA-seq immunization atlas to stabilize the evidence lower bound loss. The ROSMAP FCX snRNA-seq atlas was used to deconvolute ST spots across all regions, while our in-house-created scRNA-seq immunization atlas was used to deconvolute ST spots in gray matter. The proportion of genes expressed per ST spot (CDR) was calculated from raw counts and standardized. ST spots were deconvoluted using the resulting reference signatures, with standardized CDR as a continuous covariate and sample ID as the batch key in the `C2L` model. The model was trained in batches of 2,500 ST spots over 1,000 epochs

to stabilize the evidence lower bound loss. To account for technical variability in RNA detection sensitivity, the `detection_alpha` parameter was set to 20, and the `N_cells_per_location` parameter was set to 7 based on manual cell counts of several ST spots. The 5% quantile of the posterior distribution was computed directly and used for downstream analysis.

Defining cell-type-enriched ST spots

To identify ST spots enriched for specific cell types, we applied cell-type-specific region restrictions and thresholds to `C2L` predictions, with enrichment defined separately for each sample. For cell types from the snRNA-seq reference atlas, ST spots enriched for fibroblasts, pericytes, peripheral immune cells, smooth muscle cells and endothelial cells were annotated when `C2L` predictions for a given ST spot were in the top 1% of gray and white matter or the top 5% of meningeal ST spots. Microglia and astrocytes were considered enriched in the top 5% of gray or the top 5% of white matter. Interneuron enrichment was defined in the top 5% of gray matter, while `MYO16` ENs were enriched in the top 1% of gray matter. Oligodendrocyte precursor cells were enriched in the top 5% of both gray and white matter, and oligodendrocytes were considered enriched in the top 30% of white matter. Enrichment for layer-specific neurons was determined within the relevant cortical layers: L2/3 ENs in the top 10% of layers II–III; L4 ENs in the top 50% of layer IV; L4/5 ENs in the top 15% of layers IV–VI; and L5, L5/6, L5/6 CCa and L5/6 CCb ENs in the top 5% of layers V–VI. Layer I was excluded from enrichment analysis for all cell types in the snRNA-seq atlas. For microglia clusters from our in-house scRNA-seq immunization atlas, enrichment was defined by a sample-specific `C2L` prediction threshold set at three standard deviations above the mean in gray matter ST spots.

Definition of A β enrichment groups

ST spots were classified as A β -rich if the coverage within the expanded A β niche, indicated by barcode fluorescence intensity, exceeded a threshold of 183. The A β niche was defined to include A β -rich ST spots along with their first-order and second-order spatial neighbors in gray and white matter, based on array coordinates, covering an approximate radius of 200 μm . ST spots containing CAA pathology, as well as ST spots immediately adjacent to those, were excluded from the cortical A β niche. ST spots with unreliable A β staining, arising from technical issues or tissue anomalies such as folds or holes, were omitted from A β niche analyses.

DEG analysis

To identify DEGs across various regions of interest within our datasets, we used two distinct differential expression techniques: `DESeq2` (ref. 56) and `MAST`²⁹. Each approach was adapted to suit the specific characteristics and requirements of the comparison, considering the nature of the data (pseudobulk for `DESeq2` and single-cell method for `MAST`) and the level at which covariates were standardized (sample level for `DESeq2` and ST spot or cell level for `MAST`). Covariate selection was guided by variance partition analysis, which identified gDNA as the primary driver of variance after the experimental group. Additionally, we accounted for the number of genes expressed in a subset of ST spots or cells to control for differences in quality and sequencing depth. Sex and age were included due to their known effects on immune responses in AD. Additionally, manually annotated regions or cortical layer annotations per ST spot were incorporated where applicable to address sampling variability across anatomical areas.

DESeq2. `DESeq2` was initiated by subsetting the data for ST spots within the region of interest (ROI). Continuous covariates at the sample level, including age, average nFeatures within subsampled ST spots and gDNA percentage, were standardized within each ROI. We then filtered out genes not expressed in at least 1% of either comparison group based on raw counts, excluding genes starting with RPS, RPL, MT or HB. Pseudobulk data were created by summing raw counts by

donor to facilitate a more robust differential expression analysis. The DESeq2 analysis was conducted with the inclusion of covariates such as sex, age, average features within subsampled ST spots and gDNA percentage, all of which were standardized, if continuous. The DESeq function was run with `fitType = 'local'` to estimate dispersions using local regression, the results function was run with `independentFiltering = FALSE` to include low-expression genes in statistical testing, and LFC shrinkage was performed by running `lfcShrink` with `type = 'apeglm'`. *P* values were adjusted using the Benjamini–Hochberg method. DEG significance thresholds were set at an adjusted *P* value of 0.05 and a \log_2 fold change of $\pm\log_2(1.5)$.

MAST. For MAST, data were subsetted to include only the ST spots or cells of interest. Sample-specific and brain region-specific downsampling was applied to ensure that no single sample contributed more than 50% of ST spots or cells within a comparison group, that the fold difference in total ST spots or cells between comparison groups did not exceed three, and that each group contained no more than 3,000 ST spots or cells. Continuous covariates at the ST spot level, including age, the CDR from recorrected SCT data and gDNA percentage per sample, were standardized within each subset of ST spots or cells. We applied PrepSCTFindMarkers on the ROI, which recorrects SCT transform counts to normalize sequencing depth across samples. SCT data (\log_{10} -transformed SCT counts) were then extracted from the Seurat object. Genes prefixed with RPS, RPL, MT or HB were excluded, and additional filtering was performed based on percentage expression within comparison groups. Genes were tested if they were expressed in 1% of both groups and in 10% of either group using SCT expression data, except for Visium HD data, where genes were tested if they were expressed in 1% of either group. The \log_2 fold change between comparison groups for the remaining genes was calculated using the Seurat `FoldChange` function. MAST was run with covariates such as sex, age, CDR, gDNA percentage, brain region and manually annotated regions or cortical layers, all of which were standardized if continuous. Sample ID, or brain region and sample ID, was included as a random effect for comparisons involving multiple samples. MAST hurdle *P* values were adjusted using the Benjamini–Hochberg method. LFC from the prior calculation was appended to the results, with significance thresholds for differential expression set at an adjusted *P* value of 0.05 and a LFC of $\pm\log_2(1.5)$.

DEP analysis

Data were first subset for the ROI, and CDR (calculated based on isotype-normalized counts) was standardized within the ROI. A negative binomial generalized linear model was used through Seurat's `FindMarkers` function for differential expression analysis on isotype-normalized counts, setting `min.pct` to 0.01, `logfc.threshold` to -Inf, and standardized CDR and manually annotated regions or cortical layers as latent variables. Raw *P* values were adjusted using the Benjamini–Hochberg method, and proteins were considered significant DEPs with adjusted *P* value less than 0.05 and magnitude of average log fold change greater than $\log_2(1.5)$.

Marker expression defining cell types or A β niche types

SCT transform-corrected counts were recorrected using PrepSCTFindMarkers, with \log_{10} -transformed (\log_{10}) corrected counts utilized in analyses. To delineate general cluster markers, the `FindMarkers` function facilitated the identification of positive marker genes through a 'one-versus-many' comparative approach, testing genes expressed in more than 25% of the cluster of interest (set to 1% for Visium HD), setting `only.pos` to TRUE and using the default Wilcoxon rank-sum test. Genes prefixed with RPS, RPL, MT or HB were excluded from testing. Marker gene selection was based on Benjamini–Hochberg-adjusted *P* values below 0.05. For the specific analysis of positive and negative markers within cortical A β niche cluster 6, `FindMarkers` was used to

compare cluster 6 against all others, allowing for both positive and negative marker detection (`only.pos = FALSE`), with `min.pct` set to 0.1 and `logfc.threshold` set to -Inf, using the default Wilcoxon test. Genes prefixed with RPS, RPL, MT or HB were excluded. Marker genes were deemed significant if they presented an adjusted *P* value under 0.05 and an average LFC exceeding $\log_2(1.5)$.

Gene-set enrichment analysis

Human MSigDB. Gene lists were analyzed using the `enrichR` package⁵⁷ with the hallmark gene-set collection from the Human MSigDB. For lists containing specifically downregulated genes, combined scores were negated. A significance threshold was set at a Benjamini–Hochberg-adjusted *P* value of 0.05.

Microglia states. Signed probability fold change was calculated for each gene as the product of the negative logarithm of the adjusted *P* value and the \log_2 fold change. Enrichment for human microglial activation states^{34,41} was assessed using the `fgsea` package, with probability fold change as the ranking metric. Custom gene sets associated with various microglial activation states were compiled from the supplementary materials provided in the referenced studies. Normalized enrichment scores were calculated, and significance was determined through permutation testing, with *P* values adjusted using the Benjamini–Hochberg method. A threshold of 0.05 was applied for adjusted *P* values, with no specific cutoff for the magnitude of NES values.

LOESS trajectory analysis

LOESS was used to identify nonlinear patterns of gene expression across the A β niche in gray matter separately for each group. SCT transform counts were readjusted through PrepSCTFindMarkers, with the logarithm of one plus the corrected counts (\log_{10}) serving as the basis for our analysis. Predictions were generated for all genes in the SCT assay. A LOESS regression of span 0.75 was fit to each gene within each group using the `LOESS` function of the `R stats` package. Predicted expression values were standardized within each group. The predicted expression trajectories across the A β niche were then subdivided into clusters, using hierarchical clustering through the `hclust` function in the `R stats` package.

CellChat

Cells were grouped by broad cell type or microglia subtype, and data were subset by treatment group. SCT transform-corrected counts were recorrected using PrepSCTFindMarkers, with \log_{10} -transformed (\log_{10})-corrected counts utilized in the analysis. `ComputeCommunProb` was run with the `population.size` parameter set to TRUE in order to account for the proportion of cells in each cell group, with a 10% truncated mean used to calculate average gene expression per cell group.

Quantification and statistical analysis

Statistical analyses were conducted primarily using R (version 4.2.3) and GraphPad Prism (version 10.2.1). In GraphPad Prism, normality and variance equality were assessed using the Shapiro–Wilk and *F* tests, respectively, to guide test selection. For two-group comparisons, we applied unpaired two-tailed Student's *t*-tests (with or without Welch's correction for unequal variances) or Mann–Whitney tests. For comparisons involving more than two groups, we used one-way ANOVA with Tukey's multiple-comparisons test, Welch's ANOVA with Dunnett's T3 multiple-comparisons test, or a Kruskal–Wallis test with Dunn's multiple-comparisons test. Relative abundances, including scRNA-seq-derived cell types, microglia clusters and A β niche clusters, were compared using paired *t*-tests. For all analyses, statistical significance was defined as *P* value < 0.05, with multiple testing correction applied when appropriate, using an adjusted *P* value < 0.05.

ShinyCell

Our ShinyCell app enables users to explore scRNA-seq gene expression patterns on a UMAP, conduct comparative analyses of gene expression across different groups using violin/box plots and access supplementary built-in analytical tools.

Reporting summary

Further information on research design is available in the Nature Portfolio Reporting Summary linked to this article.

Data availability

Spatial RNA and single-cell RNA-seq data have been deposited at the Gene Expression Omnibus under accession numbers [GSE263038](#), [GSE263034](#), [GSE263079](#) and [GSE282928](#). Any additional information required to reanalyze the data reported in this work paper is available from the corresponding author upon request. Data can be explored and requested through a central hub located at <https://sites.google.com/view/adimmunization/home>. Source data are provided with this paper.

Code availability

All code used to generate the figures in this study can be found at https://github.com/gatelabNW/AD_Immunization.

References

52. Montine, T. J. et al. National Institute on Aging-Alzheimer's Association guidelines for the neuropathologic assessment of Alzheimer's disease: a practical approach. *Acta Neuropathol.* **123**, 1–11 (2012).
53. Bennett, D. A. et al. Religious Orders Study and Rush Memory and Aging Project. *J. Alzheimers Dis.* **64**, S161–S189 (2018).
54. Arzt, M. et al. LABKIT: labeling and segmentation toolkit for big image data. *Front. Comput. Sci.* **4**, 777728 (2022).
55. Li, M. et al. DISCO: a database of Deeply Integrated human Single-Cell Omics data. *Nucleic Acids Res.* **50**, D596–D602 (2022).
56. Love, M. I., Huber, W. & Anders, S. Moderated estimation of fold change and dispersion for RNA-seq data with DESeq2. *Genome Biol* **15**, 550 (2014).
57. Kuleshov, M. V. et al. Enrichr: a comprehensive gene set enrichment analysis web server 2016 update. *Nucleic Acids Res.* **44**, W90–W97 (2016).

Acknowledgements

We thank D. Bennett (Rush University) for early access to the ROSMAP snRNA-seq dataset. We thank S. H.-Y. Chou, N. Reish, D. Chatterjee and D. Krainc (Northwestern University) for helpful discussion. We also thank B. Veire (10x Genomics) for assistance with spatial proteogenomics. We also thank the staff members of the Stanford and Northwestern Alzheimer's Disease Research Centers for their assistance acquiring nAD and NND control brain tissues under NIH P30AG066515 and P30AG072977, respectively. Finally, we thank D. Kirchenbuechler and C. M. Wai (Northwestern University) for their support. Figs. 1a,b, 3a–c and 4a and Extended Data Fig. 5k were created using [BioRender.com](#). ROSMAP is supported by P30AG10161, P30AG72975, R01AG15819, R01AG17917, U01AG46152 and U01AG61356. ROSMAP resources can be requested at

<https://www.radc.rush.edu/> and <https://www.synapse.org/>. The collection of the AN1792-immunized cases was supported by the Medical Research Council (G0501033) and Alzheimer's Research UK (ART/PG2006/4, ART-EXT2010-1) with the tissue samples obtained from the University Hospital Southampton NHS Foundation Trust as part of BRAIN UK, which is supported by Brain Tumour Research and has been established with the support of the British Neuropathological Society and the Medical Research Council. This work was further supported by Northwestern University's Center for Advanced Microscopy and a Cancer Center Support Grant (NCI CA060553) and NUSeq Core Facility, Alzheimer Nederland Impulssubsidie grant WE.06-2023-03 (to L.v.O.), Alzheimer Nederland Early Career grant WE.03-2023-08 (to L.v.O.), National Institute of Neurologic Disease and Stroke K99/R00 Pathway to Independence award NS112458 (to D.G.), Bright Focus Foundation award A2023003S (to D.G.), Alzheimer's Association 23AARG-1026607 (to D.G.) and National Institute on Aging R01AG078713 (D.G.).

Author contributions

L.v.O. conducted ST, scRNaseq and confocal imaging, led the study and wrote the manuscript. B.S., A.J.E., J.B., N.S., T.K. and J.K assisted with ST, histology and scRNaseq. A.V.F. was the lead contributor to the bioinformatics analysis, guided by L.v.O. N.S., B.M.R.A., Z.Z., L.C., M.L., H.X. and T.W. assisted with bioinformatics analysis. J.L.N. assisted with histology. P.J. and R.J.C. contributed brain tissue samples from the lecanemab case. J.A.R.N. and D.B. provided brain samples from the AN1792 trial. P.J., J. Cahan, R.V., J. Chen, J.A.R.N. and D.B. assisted with study design. D.G. conceptualized, funded and led the study and edited the manuscript.

Competing interests

J.A.R.N. has been a consultant/advisor relating to AD immunization programs for Elan Pharmaceuticals, GlaxoSmithKline, Novartis, Roche, Janssen, Pfizer, Biogen and Eisai. D.B. has been a consultant/advisor relating to AD immunization programs for Elan Pharmaceuticals and Biogen. D.G. has been a consultant/advisor relating to AD therapies for Merck and Novo Nordisk. They have no financial interest in relation to AD immunotherapy. The other authors declare no competing interests.

Additional information

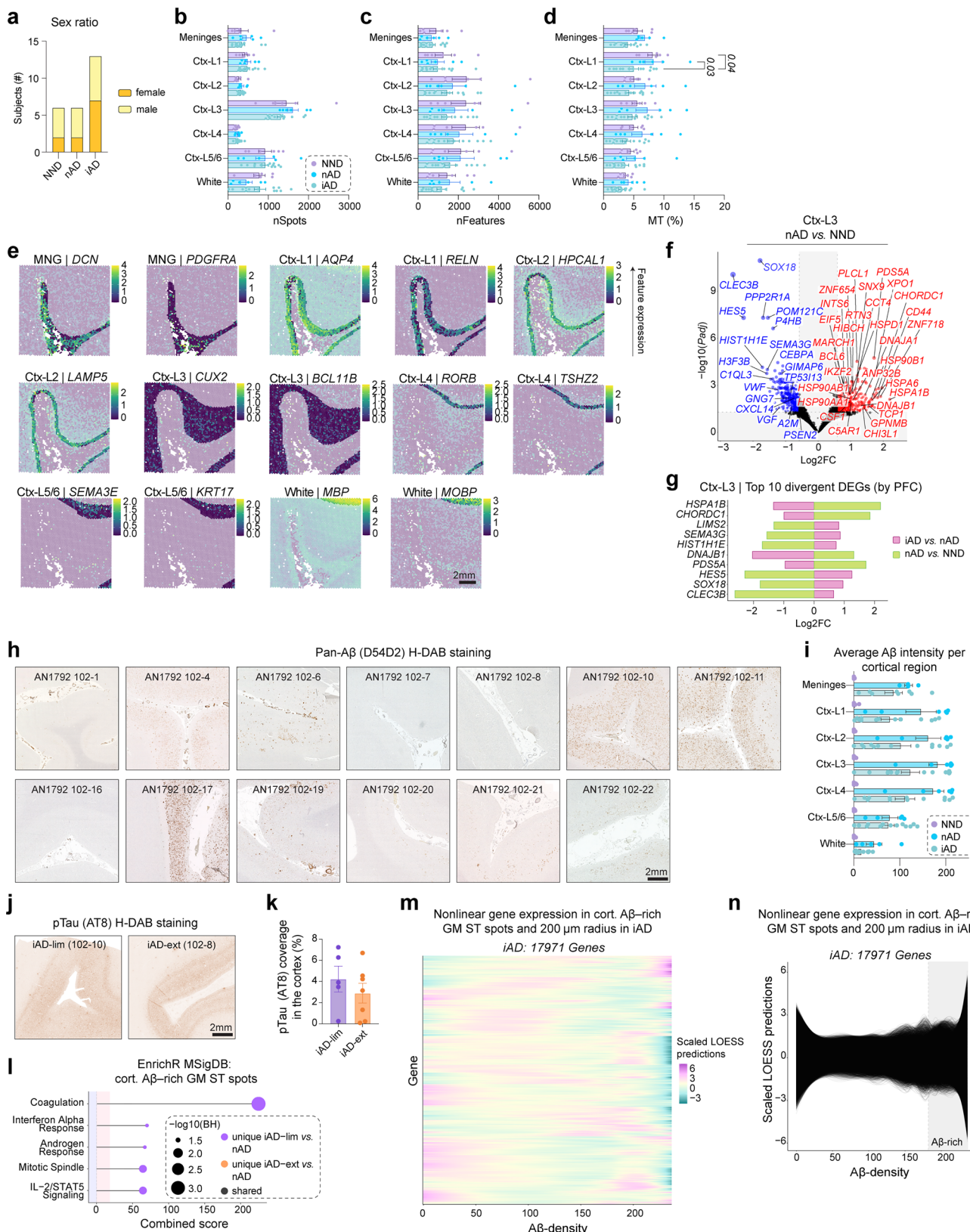
Extended data is available for this paper at <https://doi.org/10.1038/s41591-025-03574-1>.

Supplementary information The online version contains supplementary material available at <https://doi.org/10.1038/s41591-025-03574-1>.

Correspondence and requests for materials should be addressed to David Gate.

Peer review information *Nature Medicine* thanks Özgün Gökçe and the other, anonymous, reviewer(s) for their contribution to the peer review of this work. Primary Handling Editor: Jerome Staal, in collaboration with the *Nature Medicine* team.

Reprints and permissions information is available at www.nature.com/reprints.

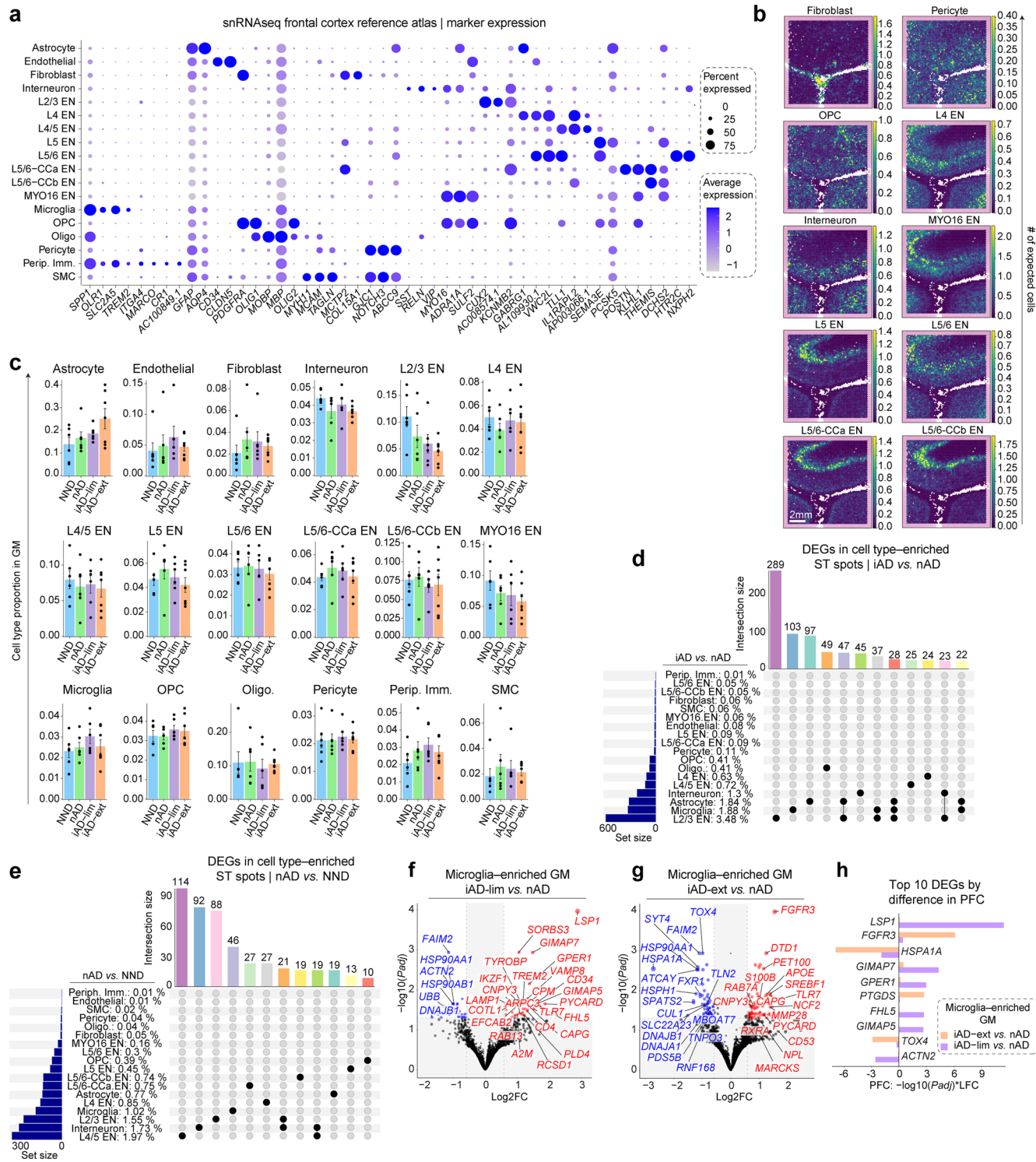


Extended Data Fig. 1 | See next page for caption.

Extended Data Fig. 1 | Active A β immunization sustains inflammation at the A β niche.

a, Sex distribution per group. **b**, Number of ST spots per manually annotated area per donor for all groups. **c**, Average number of features (genes) per spot per manually annotated area per donor for all groups. **d**, Percentages of mitochondrial gene expression per spot averaged per manually annotated area per donor for all groups. **e**, Spatial plots showing expression of brain region-specific genes overlaid on corresponding manually annotated areas (shaded). **f**, Volcano plot of DEGs in cortical layer III (nAD vs. NND). **g**, Bar plot of the top 10 divergent DEGs in cortical layer III based on PFC, comparing iAD vs. nAD and nAD vs. NND. **h**, Pan-A β (D54D2) H-DAB staining for AN1792-immunized subjects. **i**, Quantification of average A β intensity per cortical region per donor per group. **j**, Representative pTau (AT8) H-DAB staining for each group. **k**, Quantification of cortical AT8 per group. **l**, Pathway enrichment analysis of unique and shared DEGs in A β -rich gray matter ST spots (iAD-lim vs. nAD; iAD-ext vs. nAD). **m**, LOESS heatmap showing non-linear gene expression patterns relative to A β density in iAD. **n**, LOESS non-linear trajectories relative to A β density in iAD. **b-d, i, k**, Bar plots display means \pm SEM. **a-d, f-g**, NND = 6; nAD = 6; iAD = 13; iAD-lim = 6,

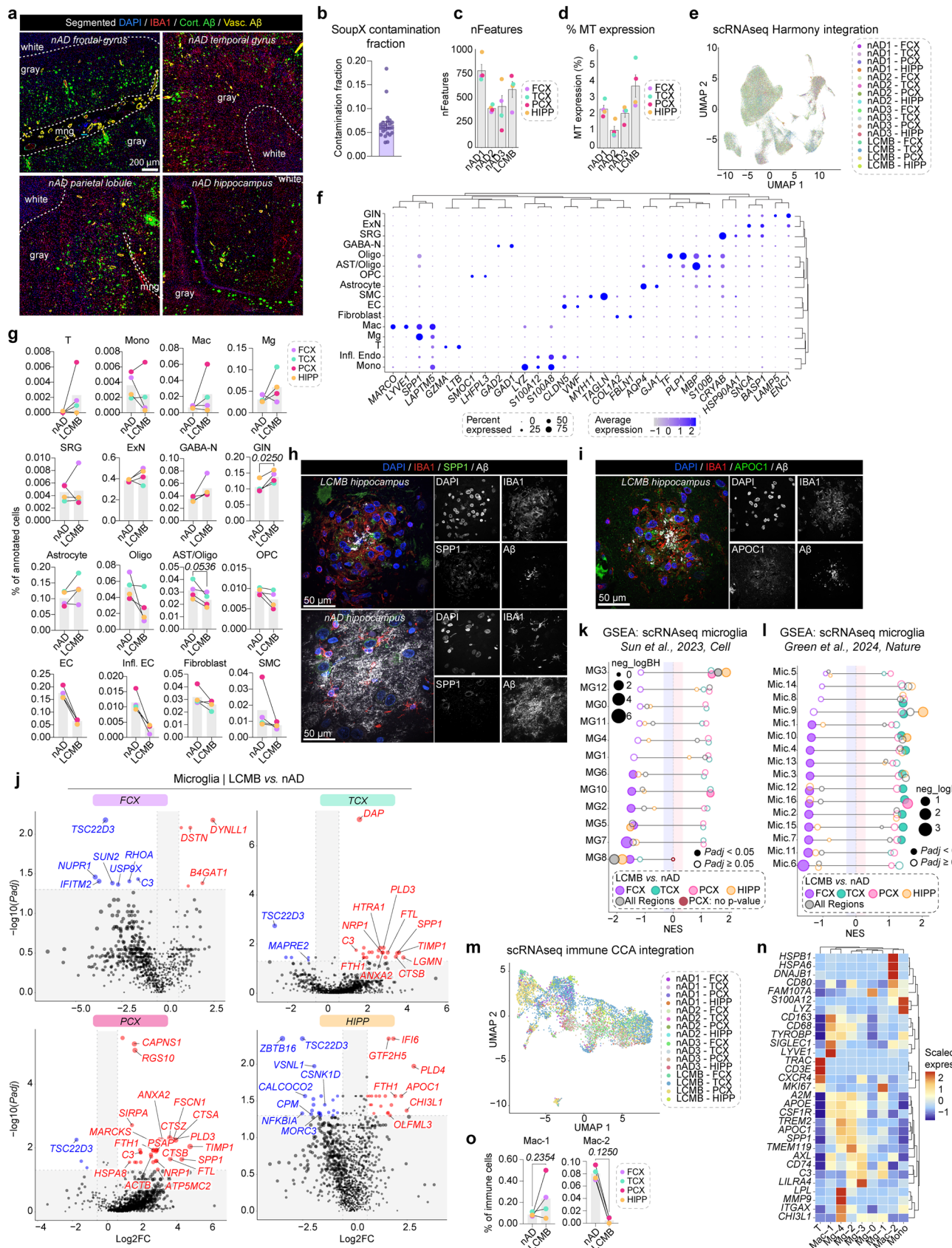
iAD-ext = 7. **i, l**, nAD = 4; iAD = 10; iAD-lim = 6, iAD-ext = 4. **k**, iAD-lim = 5, iAD-ext = 7. **l**, nAD = 4; iAD-lim = 6; iAD-ext = 4. **m-n**, iAD = 12. **f-g** DESeq2 was used to compare expression levels, with sex, age, average genes detected, and gDNA percentage included as covariates. **b-d, k**, Statistical tests, guided by Shapiro-Wilk and F tests, included t-tests, Mann-Whitney, ANOVA with Tukey's test, Welch ANOVA with Dunnett's T3 test, and Kruskal-Wallis with Dunn's test. **f-g, l**, P-values are FDR-adjusted using the Benjamini-Hochberg correction. *A β* , amyloid-beta; *AN1792-ext*, *AN1792* immunized with extensive A β clearance; *AN1792-lim*, *AN1792* immunized with limited A β clearance; *DEGs*, differentially expressed genes; *DESeq2*, Differential Expression Analysis for Sequence Count Data (version 2); *FCX*, frontal cortex; *FDR*, False Discovery Rate; *gDNA*, genomic DNA; *GM*, gray matter; *H-DAB*, Hematoxylin-3,3'-Diaminobenzidine; *iAD*, immunized Alzheimer's disease; *LCMB*, lecanemab; *LOESS*, locally estimated scatterplot smoothing; *MSigDB*, Molecular Signatures Database; *MT*, mitochondrial; *nAD*, non-immunized Alzheimer's disease; *nFeatures*, number of features; *nSpots*, number of spatial transcriptomic spots; *NND*, non-neurologic disease; *P-adj*, P-value adjusted; *PFC*, probabilistic fold change; *pTau*, phosphorylated tau; *ST*, spatial transcriptomics.



Extended Data Fig. 2 | See next page for caption.

Extended Data Fig. 2 | Microglial phenotypes define varying degrees of A β clearance. **a**, Bubble plot heatmap showing top markers expressed by cell types in the reference atlas. **b**, Spatial plots displaying the abundance of deconvoluted cell types. **c**, Bar graphs showing the proportion of deconvoluted cell types in gray matter per donor, per group. Statistical tests, guided by Shapiro–Wilk and F tests, included ANOVA with Tukey’s test, Welch ANOVA with Dunnett’s T3 test, and Kruskal–Wallis with Dunn’s test. **d**, UpSet plot indicating unique and shared DEGs in deconvoluted cell types for iAD vs. nAD. **e**, UpSet plot showing unique and shared DEGs in deconvoluted cell types for nAD vs. NND. **f–g**, Volcano plot of DEGs in microglia-enriched spots in: **f**, iAD-lim vs. nAD; and **g**, iAD-ext vs. nAD. **h**, Bar plot of the top 10 most divergent DEGs in microglia-enriched ST spots based on PFC, comparing iAD-lim vs. nAD and iAD-ext vs. nAD. Adjusted P-values used to calculate PFC are derived from DESeq2. **c**, Bar plots display means \pm SEM. **a**, 424 ROSMAP DLPFC samples. **c–h**, NND = 6; nAD = 6; iAD = 13; iAD-lim = 6; iAD-ext

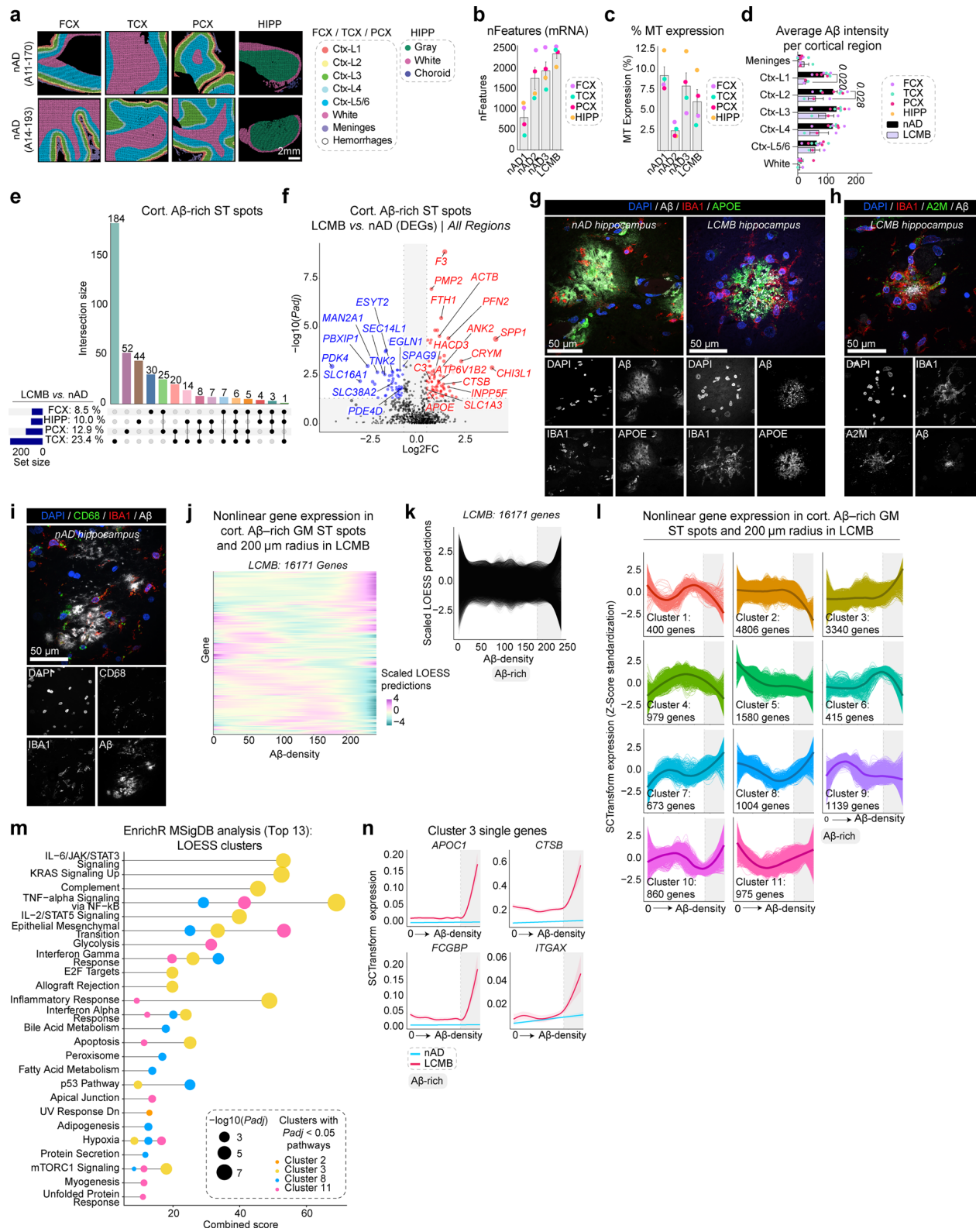
= 7. **d–h**, DESeq2 was used to compare expression levels, with sex, age, average genes detected, and gDNA percentage included as covariates. All P-values are FDR-adjusted using the Benjamini–Hochberg correction. *A β* , amyloid-beta; *AD*, Alzheimer’s disease; *AN1792-ext*, *AN1792* immunized with extensive *A β* clearance; *AN1792-lim*, *AN1792* immunized with limited *A β* clearance; *DEGs*, differentially expressed genes; *DESeq2*, Differential Expression Analysis for Sequence Count Data (version 2); *DLPFC*, dorsolateral prefrontal cortex; *EN*, excitatory neuron; *FDR*, False Discovery Rate; *gDNA*, genomic DNA; *GM*, gray matter; *iAD*, immunized Alzheimer’s disease; *L*, layer; *LCMB*, lecanemab; *nAD*, non-immunized Alzheimer’s disease; *NND*, non-neurologic disease; *oliog.*, oligodendrocyte; *OPC*, oligodendrocyte precursor cell; *P-adj*, *P*-value adjusted; *periph. imm.*, peripheral immune cell; *PFC*, probabilistic fold change; *ROSMAP*, Religious Orders Study and Rush Memory and Aging Project; *SEM*, standard error of the mean; *SMC*, smooth muscle cell; *snRNA-seq*, single-nucleus RNA sequencing; *ST*, spatial transcriptomics.



Extended Data Fig. 3 | See next page for caption.

Extended Data Fig. 3 | Passive A β immunization induces distinct microglial states. **a**, Representative confocal images showing segmented A β burden and microgliosis in regions of the nAD control patient's brain. **b**, SoupX contamination fraction for each scRNA-seq sample. **c**, Average number of features (genes) per cell per donor. **d**, Percentages of mitochondrial gene per cell averaged per donor. **e**, Integrated scRNA-seq dataset showing all analyzed cells from nAD controls and lecanemab case. **f**, Bubble plot heatmap of top markers expressed by cell types in the scRNA-seq dataset. **g**, Changes in percentages of total annotated cells for each cell type. **h**, Confocal images showing SPP1 $^+$ IBA1 $^+$ myeloid cells surrounding A β deposits in the hippocampus of the lecanemab-treated patient, absent in the nAD control. **i**, Confocal images showing APOC1 $^+$ IBA1 $^+$ myeloid cells surrounding A β deposits in the hippocampus of the lecanemab-treated patient. **j**, Volcano plot of DEGs from scRNA-seq microglia (lecanemab vs. nAD) in FCX (top left), TCX (top right), PCX (bottom left), and HIPP (bottom right). **k-l**, Pathway enrichment analysis of predefined microglial states from **k**, Sun et al.⁴¹, and **l**, Green et al.³⁴, using genes ranked by PFC in scRNA-seq regional microglia (lecanemab vs. nAD). **m**, UMAP showing reintegrated scRNA-seq immune cells for each brain region in the lecanemab case and nAD controls. **n**, Marker genes for each immune cell cluster. **o**, Percentages of each macrophage cluster. **b-d**, Bar plots display means \pm SEM. **g-o**, Bar plots display

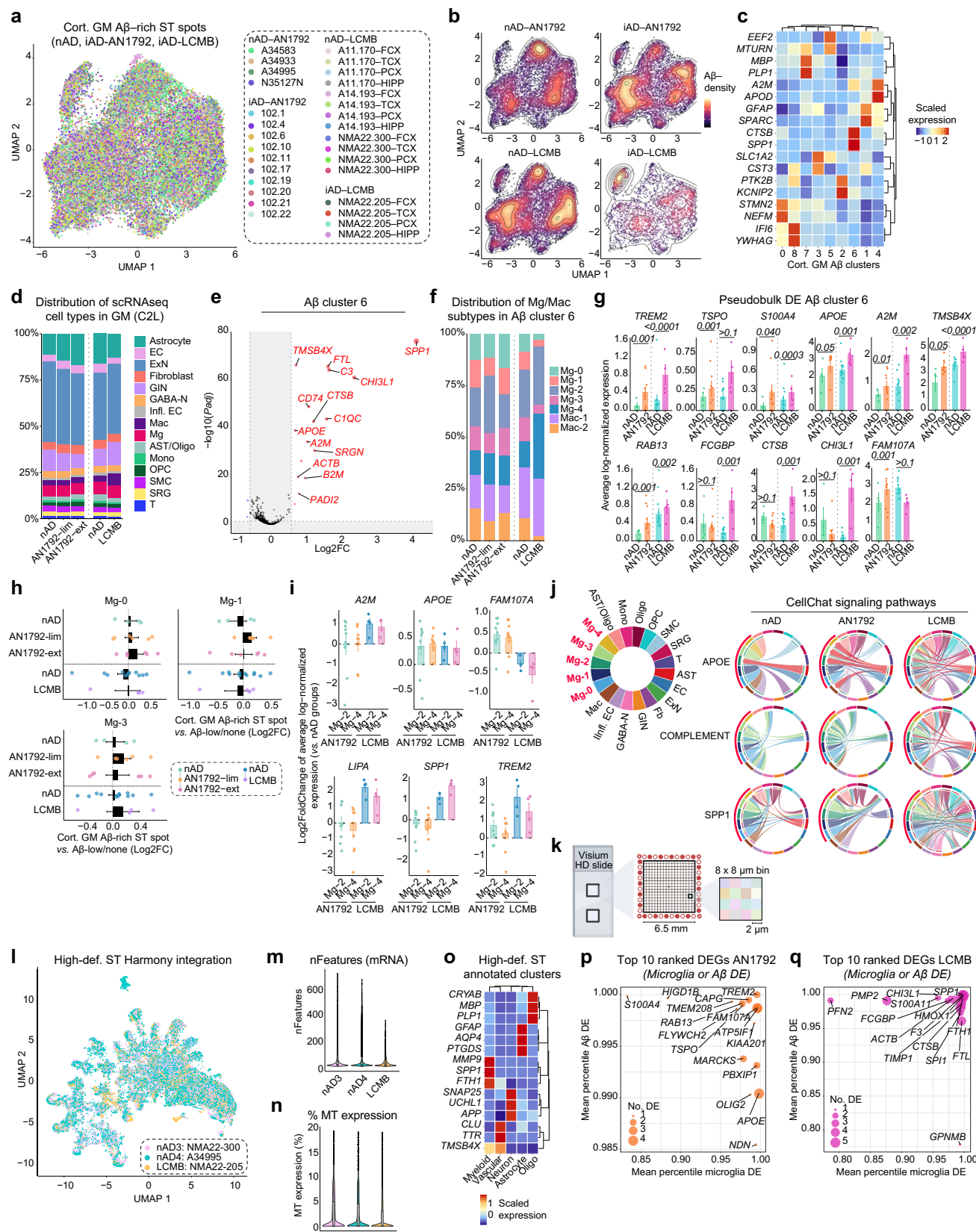
means. **b-e, g-j-o**, nAD = 3; LCMB = 1. **j-l**, MAST was used to compare expression levels, with CDR as a covariate and brain region *sample ID included as a random effect. **c-d, g, o**, Statistical tests, guided by Shapiro-Wilk and F tests, included t-tests, Mann-Whitney, ANOVA with Tukey's test, Welch ANOVA with Dunnett's T3 test, and Kruskal-Wallis with Dunn's test. **j-l**, P-values are FDR-adjusted using the Benjamini-Hochberg correction. A β , amyloid-beta; AD, Alzheimer's disease; APOC1, apolipoprotein CI; Ast, astrocyte; CCA, canonical correlation analysis; CDR, Cellular Detection Rate; DEGs, differentially expressed genes; EC, endothelial cells; ExN, excitatory neuron; FCX, frontal cortex; FDR, False Discovery Rate; GABA-N, GABAergic neuron; gDNA, genomic DNA; GIN, GABAergic interneuron; HIPP, hippocampus; IBA1, ionized calcium-binding adapter molecule 1; Infl. EC, inflamed endothelial cells; LCMB, lecanemab; Mac, macrophages; MAST, Model-based Analysis of Single-cell Transcriptomics; Mg, microglia; Mono, monocytes; MT, mitochondrial; nAD, non-immunized Alzheimer's disease; nFeatures, number of features; Oligo, oligodendrocyte; OPC, oligodendrocyte precursor cell; P-adj, P-value adjusted; PCX, parietal cortex; PFC, probabilistic fold change; scRNA-seq, single-cell/fixed RNA sequencing; SEM, standard error of the mean; SMC, smooth muscle cell; SPP1, secreted phosphoprotein 1; SRG, stress-responsive glia; ST, spatial transcriptomics; TCX, temporal cortex; UMAP, uniform manifold approximation and projection; Vasc., vascular.



Extended Data Fig. 4 | See next page for caption.

Extended Data Fig. 4 | Spatial proteogenomics links the A β niche to microglial states. **a**, Manual annotations of analyzed brain regions. **b**, Average number of features (genes) per spot per manually annotated area per donor. **c**, Percentages of mitochondrial gene expression per spot averaged per manually annotated area per donor. **d**, Quantification of average A β intensity per cortical region per donor per group. **e**, UpSet plot indicating unique and shared DEGs in cortical A β -rich ST spots in FCX, TCX, PCX and HIPP for lecanemab vs. nAD. **f**, Volcano plot of DEGs from A β -rich gray matter ST spots (lecanemab vs. nAD) across all regions. **g**, Confocal images showing IBA1 $^{+}$ myeloid cells surrounding A β deposits that colocalize with APOE in the hippocampus of the lecanemab-treated patient, with reduced IBA1 $^{+}$ recruitment in the nAD control. **h**, Confocal images showing A2M $^{+}$ IBA1 $^{+}$ myeloid cells surrounding A β deposits in the hippocampus of the lecanemab-treated patient. **i**, Confocal images showing CD68 $^{+}$ IBA1 $^{+}$ myeloid cells surrounding A β deposits in the hippocampus of the nAD control. **j**, LOESS heatmap showing non-linear gene expression patterns relative to A β density in lecanemab. **k**, LOESS non-linear trajectories relative to A β density in lecanemab. **l**, LOESS plots showing clusters of non-linear gene expression patterns relative to A β density in lecanemab. Dark line representing the mean LOESS predicted expression for the cluster and single lines indicating LOESS predicted gene expression per cluster. **m**, Pathway enrichment analysis of genes in non-linear expression clusters associated with A β density in lecanemab. **n**, LOESS plots of selected genes in LOESS cluster 3. Dark line indicating the LOESS predicted

expression and light shading representing standard error of the estimated values. **b-d**, Bar plots display means \pm SEM. nAD1, nAD2, and nAD3 each refer to separate samples. **b-f,j-n**, nAD = 3, LCMB = 1. **e-f**, MAST was used to compare expression levels. Covariates included manually annotated region or cortical layer, CDR and gDNA percentage with brain region * sample ID as a random effect (**e**) manually annotated region or cortical layer, CDR, gDNA percentage and brain region with brain region * sample ID as a random effect (**f**). **b-d**, Statistical tests, guided by Shapiro-Wilk and F tests, included t-tests, Mann-Whitney, ANOVA with Tukey's test, Welch ANOVA with Dunnett's T3 test, and Kruskal-Wallis with Dunn's test. **f, m**, P-values are FDR-adjusted using the Benjamini-Hochberg correction. A2M, alpha-2-macroglobulin; A β , amyloid-beta; AD, Alzheimer's disease; APO, apolipoprotein; APOC1, apolipoprotein C1; APOE, apolipoprotein E; CDR, Cellular Detection Rate; CD68, cluster of differentiation 68; Cort., cortical; Ctx, cortex; CTSB, cathepsin B; DEGs, differentially expressed genes; DESeq2, Differential Expression Analysis for Sequence Count Data (version 2); FCGBP, Fc fragment of IgG binding protein; FDR, False Discovery Rate; gDNA, genomic DNA; GM, gray matter; IBA1, ionized calcium-binding adapter molecule 1; ITGAX, integrin subunit alpha X; L, layer; LCMB, lecanemab; LOESS, locally estimated scatterplot smoothing; MAST, Model-based Analysis of Single-cell Transcriptomics; MSigDB, Molecular Signatures Database; MT, mitochondrial; nAD, non-immunized Alzheimer's disease; nFeatures, number of features; P-adj, P-value adjusted; SPP1, secreted phosphoprotein 1; ST, spatial transcriptomics.



Extended Data Fig. 5 | See next page for caption.

Extended Data Fig. 5 | Shared microglial response drives A β clearance after immunization. **a**, UMAP showing cortical A β -rich ST spots based on gene and protein expression, colored by brain region and donor. **b**, UMAP density plots for each group. **c**, Top two marker genes for each cortical A β -rich cluster. **d**, Bar plots showing C2L predictions of scRNA-seq cell types proportionally in the gray matter per group. **e**, Volcano plot showing DEGs distinguishing cortical A β -rich cluster 6 from all other cortical A β -rich clusters. **f**, Bar plots showing C2L predictions of scRNA-seq microglia and macrophage subtypes proportionally in A β -rich cluster 6 per group. **g**, Bar graphs showing pseudobulked *TREM2*, *TSPO*, *S100A4*, *APOE*, *A2M*, *TMSB4X*, *RAB13*, *FCGBP*, *CTSB*, *CHI3L1*, and *FAM107A* expression in A β -rich cluster 6. Error bars indicate SEM. P-values are from DESeq2. **h**, Bar plots showing log₂ fold-change in predicted abundance of deconvoluted scRNA-seq microglia types in A β -rich ST spots versus the rest in AN1792, nAD, and the lecanemab case. **i**, Bar plots showing log₂ fold-change in pseudobulked expression of *A2M*, *APOE*, *FAM107A*, *LIPA*, *SPP1*, and *TREM2* in A β -associated Mg2-enriched and Mg4-enriched ST spots compared to the nAD control group for AN1792 and the lecanemab case. **j**, Chord plots showing inferred CellChat cell-cell communication of APOE, complement, and SPP1 signaling pathways among different scRNA-seq cell types. The width of the chords reflects the strength of interaction or communication probability, with thicker chords indicating stronger signaling. **k**, Visium HD ST method. Created using BioRender.com. **l**, UMAP showing annotated binned nuclei from the high-definition ST assay, colored by donor. **m**, Number of features (genes) per binned nuclei in high-definition ST data per donor. **n**, Percentage of mitochondrial genes per binned nuclei in high-definition ST data per donor. **o**, Top three marker genes for overarching cell types annotated in the high-definition ST data. **p-q**,

Top 10 upregulated response DEGs in microglia or A β DE ranked by their average percentile in A β (Y-axis) and microglia (X-axis) DE: **o**, in AN1792; **r**, in lecanemab. **g-h-i**, Bar plots display means \pm SEM. **m-n**, Violin plots showing the data range and median. Points represent individual cells. nAD3 and nAD4 refer to separate samples. **a-c, e-f, nAD-AN1792 = 4**; iAD-lim = 6; iAD-ext = 4; nAD-LCMB = 3; LCMB = 1. **d**, nAD-AN1792 = 6; iAD-lim = 6; iAD-ext = 7; nAD-LCMB = 3; LCMB = 1. **g, nAD-AN1792 = 4**; iAD = 10; nAD-LCMB = 3; LCMB = 1. **h**, nAD-AN1792 = 4; iAD-lim = 6; iAD-ext = 6; nAD-LCMB = 3; LCMB = 1. **i**, iAD = 9 (Mg-2), 10 (Mg-4); LCMB = 1. **j**, iAD = 5; nAD = 3; LCMB = 1. **l-o**, nAD = 2; LCMB = 1. **g**, DESeq2 was used to compare expression levels. Covariates included sex, age, average genes detected, gDNA percentage (AN1792 vs. nAD); average genes detected, brain region, gDNA percentage (LCMB vs. nAD). **h**, Statistical tests, guided by Shapiro-Wilk and F tests, included t-tests, Mann-Whitney, ANOVA with Tukey's test, Welch ANOVA with Dunnett's T3 test, and Kruskal-Wallis with Dunn's test. All P-values are FDR-adjusted using the Benjamini-Hochberg correction. *A2M*, alpha-2-macroglobulin; *A β* , amyloid-beta; *AD*, Alzheimer's disease; *APOC1*, apolipoprotein C1; *APOE*, apolipoprotein E; *CD68*, cluster of differentiation 68; *Cort.*, cortical; *Ctx*, cortex; *CTSB*, cathepsin B; *DEGs*, differentially expressed genes; *DESeq2*, Differential Expression Analysis for Sequence Count Data (version 2); *FDR*, False Discovery Rate; *FCGBP*, Fc fragment of IgG binding protein; *GM*, gray matter; *HD*, high-definition; *IBAI*, ionized calcium-binding adapter molecule 1; *ITGAX*, integrin subunit alpha X; *L*, layer; *LCMB*, lecanemab; *LOESS*, locally estimated scatterplot smoothing; *MSigDB*, Molecular Signatures Database; *MT*, mitochondrial; *nAD*, non-immunized Alzheimer's disease; *nFeatures*, number of features; *P-adj*, P-value adjusted; *SPP1*, secreted phosphoprotein 1; *ST*, spatial transcriptomics.

Extended Data Table 1 | AN1792 cohort demographics

Case	Brain Region	Group ID	Neuropathological diagnosis	Origin	AD neuropathological change	Age at death (years)	Sex (m/f)	Additional findings	APOE4 allele copy number	Braak stages	AN1792 specifics							
											AN1792 dose (µg)	Number of Injections	Anti-AN1792 mean titre	Histological evidence of plaque removal Method 1	AB plaque score Method 2 (CERAD-adapted)	Duration of dementia (years)	Last known dementia status	Survival time from first immunization (months)
A18,148	FCX	NND	NND	Northwestern Pathology	NA	82	f	--	1	--	--	--	--	--	--	--	--	--
A34285	FCX	NND	NND	Stanford ADRC	NA	75	m	--	N/A	--	--	--	--	--	--	--	--	--
A34291	FCX	NND	NND	Stanford ADRC	NA	63	m	Mild-atherosclerosis	1	--	--	--	--	--	--	--	--	--
A34717	FCX	NND	NND	Stanford ADRC	NA	79	m	--	1	--	--	--	--	--	--	--	--	--
A34992	FCX	NND	NND	Stanford ADRC	NA	68	m	--	1	--	--	--	--	--	--	--	--	--
AX21,92	FCX	NND	NND	Northwestern Pathology	NA	82	f	--	1	--	--	--	--	--	--	--	--	--
A34583	FCX	nAD	AD	Stanford ADRC	A3-B3-C2	89	m	Hippocampal-CA1-TDP-42-type-A	1	--	--	--	--	--	--	--	--	--
A34644	FCX	nAD	AD	Stanford ADRC	A1-B2-C2	80	f	Mild-non-AD-tauopathy	1	--	--	--	--	--	--	--	--	--
A34933	FCX	nAD	AD	Stanford ADRC	A3-B3-C3	80	m	--	1	--	--	--	--	--	--	--	--	--
A34995	FCX	nAD	AD	Stanford ADRC	A3-B3-C3	65	f	--	1	--	--	--	--	--	--	--	--	--
A35038	FCX	nAD	AD	Stanford ADRC	A3-B3-C2	88	m	--	1	--	--	--	--	--	--	--	--	--
N35127N	FCX	nAD	AD	Stanford ADRC	A1-B3-C2	76	m	--	1	--	--	--	--	--	--	--	--	--
102,10	FCX	iAD-lim (AN1792)	AD	AN1792, Elan Pharmaceuticals	A3-B3-C3	88	f	None	0	4/5	50	7	137	+	2,9	11	Moderate	86
102,11	FCX		AD	AN1792, Elan Pharmaceuticals	A3-B3-C2	88	m	Severe-CAA	1	4/5	50	8	142	+	2,3	12	Moderate	94
102,17	FCX	iAD-lim (AN1792)	AD	AN1792, Elan Pharmaceuticals	A3-B3-C3	86	f	Small-old-right-parietal-infarct-microvascular-lesions-entorhinal-cortex	2	4/5	50	N/A	0	+	2,7	13	Severe	141
102,19	FCX		AD	AN1792, Elan Pharmaceuticals	A3-B3-C3	75	f	Severe-CAA	2	4/5	50	8	221	-	2,1	19	Severe	162
102,22	FCX	iAD-lim (AN1792)	AD	AN1792, Elan Pharmaceuticals	A3-B3-C3	74	m	Extensive-capCAA	2	4/5	225	N/A	1313	+	2,3	18	Severe	184
102,4	FCX		AD	AN1792, Elan Pharmaceuticals	A3-B3-C3	71	f	Severe-CAA	0	4/5	225	8	4072	+	1,5	10	Severe	44
102,1	FCX	iAD-ext (AN1792)	AD	AN1792, Elan Pharmaceuticals	A3-B3-C3	74	f	Numerous-cortical-microvascular-lesions-related-to-severe-CAA-meningoencephalitis	1	4/5	50	5	119	++	0,7	6	Severe	20
102,16	FCX	iAD-ext (AN1792)	AD	AN1792, Elan Pharmaceuticals	A3-B3-C0	89	f	Extensive-capCAA-small-acute-infarct-left-basal-ganglia	1	4/5	225	6	142	+++	0,4	15	Severe	111
102,20	FCX	iAD-ext (AN1792)	AD	AN1792, Elan Pharmaceuticals	A3-B3-C2	82	m	Extensive-capCAA	1	4/5	225	3	430	+++	1	17	Severe	166
102,21	FCX	iAD-ext (AN1792)	AD	AN1792, Elan Pharmaceuticals	A3-B3-C1	87	f	Extensive-capCAA	1	4/5	50	8	3045	+++	0,6	18	Severe	173
102,6	FCX	iAD-ext (AN1792)	AD	AN1792, Elan Pharmaceuticals	A3-B3-C3	81	m	Severe-CAA	1	4/5	50	8	1707	++	1,6	7	Severe	57
102,7	FCX		AD	AN1792, Elan Pharmaceuticals	A1-B3-C0	82	m	--	1	4/5	50	8	4374	+++	0,05	6	Severe	60
102,8	FCX	iAD-ext (AN1792)	AD	AN1792, Elan Pharmaceuticals	A1-B3-C1	63	m	--	1	4/5	50	8	6470	+++	0,5	10	Severe	64

A β , amyloid-beta; AD, Alzheimer's disease; ADRC, Alzheimer's Disease Research Center; APOE, apolipoprotein E; CAA, cerebral amyloid angiopathy; capCAA, capillary cerebral amyloid angiopathy; CERAD, Consortium to Establish a Registry for Alzheimer's Disease, classification of neuritic plaque pathology in AD; CVA, cerebrovascular accident; DVT, deep vein thrombosis; FTLD-TDP, frontotemporal lobar degeneration with TAR DNA-binding protein 43 pathology; LBD, Lewy body disease, neocortical (diffuse); PSP, progressive supranuclear palsy; VBI, vascular brain injury; FCX, frontal cortex; iAD-lim, immunized with limited A β clearance; iAD-ext, immunized with extensive A β clearance; m/f, male/female; NA, not available/applicable; nAD, non-immunized Alzheimer's disease; NND, non-neurologic disease; TDP-43, TAR DNA-binding protein 43; Anti-AN1792 mean titre, mean antibody titre against AN1792; Braak stages, classification of tau pathology in AD; APOE allele copy number, number of APOE- ϵ 4 alleles; duration of dementia, duration in years; last known dementia status, severity at last assessment; survival time from first immunization, months from first AN1792 dose to death. Method 1: Analysis of plaque removal was scored semi-quantitatively in frontal, temporal, parietal and occipital neocortex as: very extensive (that is nearly complete clearance of plaques) = +++; intermediate (that is multiple and/or extensive plaque-free foci each involving a >1 cm length of cortical ribbon) = ++; very limited (that is single and/or small plaque-free foci each involving each involving a <1 cm length of cortical ribbon) = +; no evidence of plaque removal = -. Method 2: Quantification of amyloid- β plaques in coronal hemisphere sections (score out of 3). *LBD with marked capillary angiopathy but no plaques, possibly reflecting clearance of diffuse plaques. Alzheimer's disease neuropathological change: A = amyloid- β plaque score; B = neurofibrillary tangle stage; C = neuritic plaque score according to National Institute on Aging-Alzheimer's Association guidelines (Hyman et al., 2012).

Extended Data Table 2 | Lecanemab cohort demographics

Spatial proteogenomics and single-cell RNA sequencing										
Case	Brain Region(s)*	Group ID	Figure ID	Neuropathological diagnosis	Origin	Age at death (years)	Sex (m/f)	Additional notes		APOE4 allele copy number
NMA22-205	FCX, TCX, PCX, HIPP	LCMB	LCMB	AD	Northwestern Pathology	65	f	Participated in phase III trial of lecanemab, received three lecanemab infusions over the course of five weeks. Developed acute ischemic stroke-like symptoms shortly after the final lecanemab dose and passed away days later.		2
A14-193	FCX, TCX, PCX, HIPP	nAD	nAD1	AD	Northwestern Pathology	64	f			2
A11-170	FCX, TCX, PCX, HIPP	nAD	nAD2	AD	Northwestern Pathology	66	f			2
NMA22-300	FCX, TCX, PCX, HIPP	nAD	nAD3	AD	Northwestern Pathology	82	m			2

High-definition spatial transcriptomics										
Case	Brain Region(s)*	Group ID	Figure ID	Neuropathological diagnosis	Origin	Age at death (years)	Sex (m/f)	Additional notes		APOE4 allele copy number
NMA22-205	HIPP	LCMB	LCMB	AD	Northwestern Pathology	65	f	Participated in phase III trial of lecanemab, received three lecanemab infusions over the course of five weeks. Developed acute ischemic stroke-like symptoms shortly after the final lecanemab dose and passed away days later.		2
NMA22-300	HIPP	nAD	nAD3	AD	Northwestern Pathology	82	m			2
A34995	HIPP	nAD	nAD4	AD	Stanford ADRC	65	f	--		1

*In the metadata, the brain regions are referred to by the following scheme: A indicates nAD sample while B denotes LCMB sample; region 1 is FCX, 3 is TCX, 4 is PCX, and 9 is HIPP. A β , amyloid-beta; AD, Alzheimer's disease; APOE, apolipoprotein E; APOE allele copy number, number of APOE-ε4 alleles; FCX, frontal cortex; HIPP, hippocampus; LCMB, lecanemab; m/f, male/female; NA, not available/applicable; nAD, non-immunized Alzheimer's disease; PCX, parietal cortex; TCX, temporal cortex; TDP-43, TAR DNA-binding protein 43; Stanford ADRC, Stanford Alzheimer's Disease Research Center; Age at death, age in years at time of death; Additional notes, extra relevant clinical or procedural information.

Extended Data Table 3 | Antibody information

Antibody information						
Target	Concentration	Secondary	DAPI	TruBlack Plus	Antigen Retrieval	
Gt anti-APOE [ab947] Ms anti- α [D3D2N] Rb anti-Iba1 [019-19741]	Sigma Cell Signaling Wako	1:500 1:1000 1:500	Dk anti-Gt 647 Dk anti-Ms 488 Dk anti-Rb 568	Invitrogen Invitrogen Invitrogen	1:5000	1:40
Ms anti-CD68 [KP1] Rb anti- α [D54D2] Gt anti-Iba1 [ab5076]	Abcam Cell Signaling Abcam	1:400 1:1000 1:150	Dk anti-Ms 488 Dk anti-Rb 647 Dk anti-Gt 568	Invitrogen Invitrogen Invitrogen	1:5000	1:40
Rb anti-TMS1/ASC [RM1049] Ms anti- α [4G8] Gt anti-Iba1 [ab5076]	Abcam BioLegend Abcam	1:100 1:500 1:100	Dk anti-Rb 594 Dk anti-Ms 647 Dk anti-Gt 488	Invitrogen Invitrogen Invitrogen	1:5000	1:40
Rb anti-A2M [EPR4432] Ms anti- α [4G8] Gt anti-Iba1 [ab5076]	Abcam BioLegend Abcam	1:250 1:500 1:100	Dk anti-Rb 594 Dk anti-Ms 647 Dk anti-Gt 488	Invitrogen Invitrogen Invitrogen	1:5000	1:40
Rb anti-APOC1 [EPR16813] Ms anti- α [4G8] Gt anti-Iba1 [ab5076]	Abcam BioLegend Abcam	1:200 1:500 1:100	Dk anti-Rb 594 Dk anti-Ms 647 Dk anti-Gt 488	Invitrogen Invitrogen Invitrogen	1:5000	1:40
Rb anti-SPP1 [ab8448] Ms anti- α [4G8] Gt anti-Iba1 [ab5076]	Abcam BioLegend Abcam	1:100 1:500 1:100	Dk anti-Rb 594 Dk anti-Ms 647 Dk anti-Gt 488	Invitrogen Invitrogen Invitrogen	1:5000	1:40

Reporting Summary

Nature Portfolio wishes to improve the reproducibility of the work that we publish. This form provides structure for consistency and transparency in reporting. For further information on Nature Portfolio policies, see our [Editorial Policies](#) and the [Editorial Policy Checklist](#).

Statistics

For all statistical analyses, confirm that the following items are present in the figure legend, table legend, main text, or Methods section.

n/a Confirmed

- The exact sample size (n) for each experimental group/condition, given as a discrete number and unit of measurement
- A statement on whether measurements were taken from distinct samples or whether the same sample was measured repeatedly
- The statistical test(s) used AND whether they are one- or two-sided
Only common tests should be described solely by name; describe more complex techniques in the Methods section.
- A description of all covariates tested
- A description of any assumptions or corrections, such as tests of normality and adjustment for multiple comparisons
- A full description of the statistical parameters including central tendency (e.g. means) or other basic estimates (e.g. regression coefficient) AND variation (e.g. standard deviation) or associated estimates of uncertainty (e.g. confidence intervals)
- For null hypothesis testing, the test statistic (e.g. F , t , r) with confidence intervals, effect sizes, degrees of freedom and P value noted
Give P values as exact values whenever suitable.
- For Bayesian analysis, information on the choice of priors and Markov chain Monte Carlo settings
- For hierarchical and complex designs, identification of the appropriate level for tests and full reporting of outcomes
- Estimates of effect sizes (e.g. Cohen's d , Pearson's r), indicating how they were calculated

Our web collection on [statistics for biologists](#) contains articles on many of the points above.

Software and code

Policy information about [availability of computer code](#)

Data collection

During the ST workflow, tissues were imaged using an EVOS M7000 Imaging System (AMF7000, ThermoFisher Scientific) with a 20x-objective (0.45NA, AMEP4982, ThermoFisher Scientific, or Olympus Lucplanfl N 20x/0.45 Ph1 UIS2 Collar Fn22). The final spatial transcriptomic libraries were sequenced by the NUSeq Core at Northwestern University Feinberg School of Medicine using either the Illumina NovaSeq 6000 or the NovaSeq X Plus platforms. The sequencing targeted a depth of 25,000 reads per tissue-covered ST spot for gene expression libraries, 5,000 reads per spot for protein expression libraries, and 275 million reads per fully-covered capture area for Visium HD libraries; following recommended guidelines.

In the scRNAseq workflow, cells were imaged using the same EVOS M7000 Imaging System with a 4x objective lens (0.13NA, AMEP4980, ThermoFisher Scientific). The final libraries were indexed, pooled, and sequenced together at the NUSeq Core on an Illumina NovaSeq X Plus sequencer, targeting approximately 25,000 reads per cell.

Consecutive sections stained for pan-A β were imaged using a 20x-objective (0.5NA) on a TissueGnostics slide scanner at the Northwestern University Center for Advanced Microscopy.

The sequenced data were processed using 10X Space Ranger software versions 2.0.0 for ST AN1792, 2.1.1 for ST Lecanemab/nAD, and 3.0.0 for Visium HD. Additionally, 10X CellRanger version 7.2.0 was used for scRNAseq.

Data analysis

All code used to generate the figures in this study can be found at https://github.com/gatelabNW/AD_Immunization.

Imaging were analyzed and quantified using FIJI, by a researcher blinded to sample identification. Graphpad Prism version 10.2.1 was used for analyses specific to microscopy measurements and the comparison of relative abundances of scRNAseq-derived cell types and microglia

clusters, and A β niche clusters. For quality-control metrics on the sample level, we first applied Shapiro–Wilk test and F tests to evaluate normality and variance equality, informing the selection of appropriate statistical tests. The chosen tests included the unpaired two-tailed Student's t-test, with or without Welch's correction for unequal variance, as needed, and the Mann–Whitney test for non-parametric data. For comparisons of relative abundances (scRNAseq-derived cell-types, microglia clusters, and A β niche clusters), a paired t-test was utilized. To compare quality-control metrics (such as the number of features and the percentage of mitochondrial expression) between the lecanemab and nAD ST spots, an unpaired, two-sided Wilcoxon test without a continuity correction was used. Across all analyses, a P-value threshold of less than 0.05 was set to denote statistical significance.

Statistical analyses in R v4.2.3 primarily used the following packages: Seurat v5.1.0, sctransform v0.4.1, SoupX v1.6.2, DoubletFinder v2.0.4, MAST v1.27.1, DESeq2 v1.38.3, CellChat v2.1.2, fgsea v1.24.0, enrichR v3.2, ShinyCell v2.1.0. Analyses in R v4.2.0 used the following packages: FastIntegration v1.0.0. Analyses in python v3.9 primarily used the following packages: cell2location v0.1.3, stardist v0.9.1.

For manuscripts utilizing custom algorithms or software that are central to the research but not yet described in published literature, software must be made available to editors and reviewers. We strongly encourage code deposition in a community repository (e.g. GitHub). See the Nature Portfolio [guidelines for submitting code & software](#) for further information.

Data

Policy information about [availability of data](#)

All manuscripts must include a [data availability statement](#). This statement should provide the following information, where applicable:

- Accession codes, unique identifiers, or web links for publicly available datasets
- A description of any restrictions on data availability
- For clinical datasets or third party data, please ensure that the statement adheres to our [policy](#)

Spatial RNA/protein and single-cell RNA-seq data have been deposited at GEO under accession numbers GSE263034, GSE263038 and GSE263079. Data can be explored and requested through a central hub located at: <https://sites.google.com/view/adimmunization/home>.

Human research participants

Policy information about [studies involving human research participants and Sex and Gender in Research](#).

Reporting on sex and gender

The NND and nAD subjects were matched as closely as possible to their respective experimental groups (AN1792 and lecanemab) based on age at death and pathology, with additional matching by sex where possible. In the AN1792 group, 7 out of 13 subjects (54%) were female, compared to 2 out of 6 (33%) in the nAD control group and 2 out of 6 (33%) in the NND control group. The lecanemab sample was a 65-year-old woman, with the nAD control group consisting of 2 out of 3 women (67%). To account for variations in age and sex, all analyses included age and sex as covariates. The sex and age of each subject are consistently documented throughout the manuscript.

Population characteristics

AN1792, nAD and NND controls: Post-mortem FFPE frontal cortex samples were obtained from 13 iAD patients (mean age = 79.97 years, range = 63–89) enrolled in the AN1792 phase I trial, following previous clinical and neuropathological reporting. Frontal cortex samples from 6 nAD controls (mean age = 79.60 years, range = 65–89) and 6 NND controls (mean age = 74.93 years, range = 63–82) were included as matched controls due to limited availability of placebo-treated samples. All nAD cases and 4 NND cases were sourced from the Stanford Alzheimer's Disease Research Center, with 2 additional NND samples from Northwestern Pathology. Extended clinical and demographic data for iAD, nAD, and NND cases are provided in Extended Data Table 1.

Lecanemab and nAD controls: The lecanemab-treated case involved a 65-year-old woman with AD and significant CAA pathology, including cortical vasculitis and multifocal hemorrhage, consistent with anti-A β treatment effects. FFPE sections from frontal, temporal, parietal, and hippocampal regions were analyzed. Comparative nAD controls (mean age = 69.3 years, range = 62–82) were matched by APOE ϵ 4/ ϵ 4 genotype, CAA, and high AD pathology. Extended demographic and clinical information for lecanemab and matched nAD cases are available in Extended Data Table 1.

Recruitment

Brain tissue from AD patients enrolled in the Elan Pharmaceuticals Phase I AN1792 trial was obtained through the University of Southampton, with post-mortem examination consent provided by patients or their caretakers. Control samples for the neuropathologically confirmed AD (nAD) cases and four non-neurologic disease (NND) cases were sourced from the Stanford Alzheimer's Disease Research Center, while two additional NND samples were provided by Northwestern Pathology.

The lecanemab-treated brain sample was obtained from a 65-year-old woman with AD through Northwestern Pathology, with consent for a full-body post-mortem examination and reporting of neuropathological findings related to anti-A β treatment. For comparative purposes, her brain was evaluated against APOE ϵ 4/ ϵ 4 genotype-matched pathological nAD controls provided by Northwestern Pathology.

Ethics oversight

Collection of brain tissue was approved by the Institutional Review Board of each university.

Note that full information on the approval of the study protocol must also be provided in the manuscript.

Field-specific reporting

Please select the one below that is the best fit for your research. If you are not sure, read the appropriate sections before making your selection.

Life sciences

Behavioural & social sciences

Ecological, evolutionary & environmental sciences

For a reference copy of the document with all sections, see nature.com/documents/nr-reporting-summary-flat.pdf

Life sciences study design

All studies must disclose on these points even when the disclosure is negative.

Sample size

The pathological cohorts and samples utilized in this study are unique. Consequently, every sample of sufficient quality was included in the study. Notably, controls were matched as closely as possible in terms of age, sex and pathology. In the case of the lecanemab sample, controls were selected based on the pathological resemblance and APOE4 genotype, albeit without prior exposure to the drug.

Data exclusions

Three of the 16 AD donors (cases 102-2, 102-3, and 102-9) were excluded due to low RNA quality, yielding a final cohort of 13 iAD samples for ST analysis. RNA quality was assessed based on DV200 scores, the number of genes detected per ST spot, and the percentage of mitochondrial genes per spot. For ST analysis, spots with extreme UMI counts, low feature counts, more than 20% mitochondrial expression (or over 30% for hippocampus), or those located at the slide edges or lacking tissue coverage were removed on a per-sample basis.

For scRNAseq, cells with mitochondrial gene expression above 20% and doublets were excluded. Additionally, AN1792 donor samples 102-7, 102-8, 102-11, and 102-21 were removed due to high contamination fractions, low UMI counts, or elevated mitochondrial expression.

Replication

There are no replications of the study cohort available. However, a subset of the samples was processed twice during a pilot study to test and set up ST, resulting in consistent data outputs.

Randomization

For AN1792 ST, each iAD sample was paired with a NND or NAD control sample when possible. Typically, 2–6 samples, often four, were processed concurrently on a staggered schedule. Almost all samples were sequenced simultaneously, with the exception of one iAD and four NND samples.

In lecanemab ST, frontal and temporal cortex samples from both the lecanemab-treated patient (NMA22-205) and an nAD control (NMA22-300) were processed and sequenced together. Parietal and hippocampal samples from both the lecanemab patient and the same nAD control were also co-processed and sequenced. Two additional nAD controls (A14-193 and A11-170) were introduced later and were processed and sequenced together.

For the Visium HD processing, all samples were processed and sequenced together.

For single-cell RNA sequencing (scRNAseq), samples were processed and sequenced in batches. The first batch included four brain regions—frontal cortex, temporal cortex, parietal cortex, and hippocampus—from one nAD control (NMA22-205) and one lecanemab-treated sample (NMA22-300). The second batch included the same regions from two additional nAD controls (A14-193 and A11-170). The third batch consisted of frontal cortex samples from 10 AN1792 samples (102-1, 102-7, 102-8, 102-11, 102-15, 102-16, 102-17, 102-19, 102-21, and 102-22).

Blinding

During the ST workflow, it was not possible to identify the samples being used because the sample IDs were obscured by the cassette used in the ST process. For scRNAseq, the samples were coded to ensure unbiased analysis. Additionally, immunohistochemistry analyses were conducted by a researcher who was blinded to the group IDs.

Reporting for specific materials, systems and methods

We require information from authors about some types of materials, experimental systems and methods used in many studies. Here, indicate whether each material, system or method listed is relevant to your study. If you are not sure if a list item applies to your research, read the appropriate section before selecting a response.

Materials & experimental systems

n/a	<input type="checkbox"/> Involved in the study <input checked="" type="checkbox"/> Antibodies <input checked="" type="checkbox"/> Eukaryotic cell lines <input checked="" type="checkbox"/> Palaeontology and archaeology <input checked="" type="checkbox"/> Animals and other organisms <input checked="" type="checkbox"/> Clinical data <input checked="" type="checkbox"/> Dual use research of concern
-----	--

Methods

n/a	<input type="checkbox"/> Involved in the study <input checked="" type="checkbox"/> ChIP-seq <input checked="" type="checkbox"/> Flow cytometry <input checked="" type="checkbox"/> MRI-based neuroimaging
-----	--

Antibodies

Antibodies used

For immunofluorescent staining, primary antibodies were as follows: pan-amyloid-beta (Cell Signaling, clone D54D2, 8243, 1:1000), pan-amyloid-beta (Cell Signaling, clone D3D2N, 15126, 1:1000), pan-amyloid-beta (BioLegend, clone 4G8, 800708, 1:500), APOE (Sigma Aldrich, ab947, 1:500), CD68 (Abcam, clone KP1, ab955, 1:400), Iba1 (Abcam, ab5076, 1:150), Iba1 (WAKO, 019-19741, 1:400), TMS1/ASC (Abcam, clone RM1049, ab309497, 1:100), A2M (Abcam, clone EPR4432, ab109422, 1:250), APOC1 (Abcam, clone EPR16813, ab198288, 1:200), SPP1 (Abcam, ab8448, 1:100), and DAPI (ThermoFisher, 62248, 1:5000). Secondary antibodies were as follows: Donkey anti-Mouse 488 (Invitrogen, A32766, 1:400), Donkey anti-Rabbit 568 (Invitrogen, A10042, 1:400), Donkey anti-Goat 647 (Invitrogen, A21447, 1:400), Donkey anti-Goat 568 (Invitrogen, A11057, 1:400), Donkey anti-Rabbit 647 (Invitrogen, A31573, 1:400), Donkey anti-Rabbit 594 (Invitrogen, A21207, 1:400), Donkey anti-Mouse 647 (Invitrogen, A31571, 1:400), and Donkey anti-Goat 488 (Invitrogen, A11055, 1:400).

Validation

All antibodies are commercially available and have been tested in human samples.

Website reference:

pan-amyloid-beta (Cell Signaling, clone D3D2N, 15126, 1:1000) <https://www.cellsignal.com/products/primary-antibodies/b-amyloid-d3d2n-mouse-mab/15126>

pan-amyloid-beta (Cell Signaling, clone D54D2, 8243, 1:1000) <https://www.cellsignal.com/products/primary-antibodies/b-amyloid-d54d2-xp-rabbit-mab/8243>

pan-amyloid-beta (BioLegend, clone 4G8, 800708, 1:500)

APOE (Sigma Aldrich, ab947, 1:500) <https://www.sigmal Aldrich.com/US/en/product/mm/ab947>

CD68 (Abcam, clone KP1, ab955, 1:400) <https://www.abcam.com/products/primary-antibodies/cd68-antibody-kp1-ab955.html>

Iba1 (Abcam, ab5076, 1:150) <https://www.abcam.com/products/primary-antibodies/iba1-antibody-ab5076.html>

Iba1 (WAKO, 019-19741, 1:400) <https://labchem-wako.fujifilm.com/us/product/detail/W01W0101-1974.html>

TMS1/ASC (Abcam, clone RM1049, ab309497, 1:100) <https://www.abcam.com/en-us/products/primary-antibodies/tms1-asc-antibody-rm1049-ab309497>

A2M (Abcam, clone EPR4432, ab109422, 1:250) <https://www.abcam.com/en-us/products/primary-antibodies/alpha-2-macroglobulin-antibody-epr4432-ab109422>

APOC1 (Abcam, clone EPR16813, ab198288, 1:200) <https://www.abcam.com/en-us/products/primary-antibodies/apolipoprotein-ci-apo-ci-antibody-epr16813-ab198288>

SPP1 (Abcam, ab8448, 1:100) <https://www.abcam.com/en-us/products/primary-antibodies/osteopontin-antibody-ab8448>

DAPI (ThermoFisher, 62248, 1:5000) <https://www.thermofisher.com/order/catalog/product/62248>

Donkey anti-Mouse 488 (Invitrogen, A32766, 1:400) <https://www.thermofisher.com/antibody/product/Donkey-anti-Mouse-IgG-H-L-Highly-Cross-Adsorbed-Secondary-Antibody-Polyclonal/A32766>

Donkey anti-Rabbit 568 (Invitrogen, A10042, 1:400) <https://www.thermofisher.com/antibody/product/Donkey-anti-Rabbit-IgG-H-L-Highly-Cross-Adsorbed-Secondary-Antibody-Polyclonal/A10042>

Donkey anti-Goat 647 (Invitrogen, A21447, 1:400) <https://www.thermofisher.com/antibody/product/Donkey-anti-Goat-IgG-H-L-Cross-Adsorbed-Secondary-Antibody-Polyclonal/A-21447>

Donkey anti-Goat 568 (Invitrogen, A11057, 1:400) <https://www.thermofisher.com/antibody/product/Donkey-anti-Goat-IgG-H-L-Cross-Adsorbed-Secondary-Antibody-Polyclonal/A-11057>

Donkey anti-Rabbit 647 (Invitrogen, A31573, 1:400) <https://www.thermofisher.com/antibody/product/Donkey-anti-Rabbit-IgG-H-L-Highly-Cross-Adsorbed-Secondary-Antibody-Polyclonal/A-31573>

Donkey anti-Rabbit 594 (Invitrogen, A21207, 1:400) <https://www.thermofisher.com/antibody/product/Donkey-anti-Rabbit-IgG-H-L-Highly-Cross-Adsorbed-Secondary-Antibody-Polyclonal/A-21207>

Donkey anti-Mouse 647 (Invitrogen, A31571, 1:400) <https://www.thermofisher.com/antibody/product/Donkey-anti-Mouse-IgG-H-L-Highly-Cross-Adsorbed-Secondary-Antibody-Polyclonal/A-31571>

Donkey anti-Goat 488 (Invitrogen, A11055, 1:400) <https://www.thermofisher.com/antibody/product/Donkey-anti-Goat-IgG-H-L-Cross-Adsorbed-Secondary-Antibody-Polyclonal/A-11055>